Mon. Not. R. Astron. Soc. **000**, 1–21 (2012) Printed 29 February 2012 (MN LATEX style file v2.2)

Mechanical AGN Feedback: Controlling the Thermodynamical Evolution of Elliptical Galaxies

M. Gaspari[1⋆], F. Brighenti[1] and P. Temi[2]
[1]*Astronomy Department, University of Bologna, Via Ranzani 1, 40127 Bologna, Italy*
[2]*Astrophysics Branch, NASA/Ames Research Center, MS 245-6, Moffett Field, CA 94035*

29 February 2012

ABSTRACT
A fundamental gap in the current understanding of galaxies concerns the thermodynamical evolution of the ordinary, baryonic matter. On one side, radiative emission drastically decreases the thermal energy content of the interstellar plasma (ISM), inducing a slow cooling flow toward the centre. On the other side, the active galactic nucleus (AGN) struggles to prevent the runaway cooling catastrophe, injecting huge amount of energy in the ISM. The present study intends to deeply investigate the role of mechanical AGN feedback in (isolated or massive) elliptical galaxies, extending and completing the mass range of tested cosmic environments. Our previously successful feedback models, in galaxy clusters and groups, demonstrated that AGN outflows, self-regulated by cold gas accretion, are able to properly quench the cooling flow, without destroying the cool core. Via 3D hydrodynamic simulations (FLASH 3.3), including also stellar evolution, we show that massive mechanical AGN outflows can indeed solve the cooling flow problem for the entire life of the galaxy, at the same time reproducing typical observational features and constraints, such as buoyant underdense bubbles, elliptical shock cocoons, sonic ripples, dredge-up of metals, subsonic turbulence, and extended filamentary or nuclear cold gas. In order to avoid overheating and totally emptying the isolated galaxy, the frequent mechanical AGN feedback should be less powerful and efficient ($\epsilon \sim 10^{-4}$), compared to the heating required for more massive and bound ellipticals surrounded by the intragroup medium ($\epsilon \sim 10^{-3}$).

Key words: cooling flows – galaxies: active – galaxies: ISM – galaxies: jets – hydrodynamics – intergalactic medium – X-rays: galaxies: ellipticals.

1 INTRODUCTION

The present paper is the third of a series aimed to investigate how massive black holes (BHs) control the thermal and dynamical evolution of the gaseous component of galaxies, groups and clusters. The focus of this investigation is the effect of AGN feedback on the interstellar medium of isolated and massive elliptical galaxies.

The key role of active galactic nuclei outbursts in sterilising the parent galaxy – quenching star formation and gas cooling – has become blatant in the last decade. The need for sustained gas heating in a range of astronomical systems comes from both observations and theory. High spatial resolution X-ray and radio images of clusters, groups and elliptical galaxies reveal a clear connection between the nuclear activity and the large scale disturbances in the hot gas, such as X-ray cavities often filled with radio emission (e.g. Diehl & Statler 2008a; Dunn et al. 2010b; Giacintucci et al. 2011), and shocks (Baldi et al. 2009). These features are thought to be the manifestation of the heating process necessary to prevent the excessive gas cooling predicted by the classic cooling flow theory (Fabian 1994; Mathews & Brighenti 2003). X-ray and UV spectroscopy indicate indeed cooling rates at least one order of magnitude lower than simple expectations, both in galaxies than in clusters/groups – this is the so-called *cooling flow problem* (e.g. Peterson et al. 2001, 2003; Oegerle & Hill 2001; Xu et al. 2002; Tamura et al. 2003; Bregman et al. 2001, 2005, 2006). Excellent reviews on this subject are provided by Peterson & Fabian (2006), McNamara & Nulsen (2007), and Böhringer & Werner (2010).

Another piece of evidence for the reduced cooling rates comes from the lack of significant star formation in most massive elliptical galaxies (e.g. Ferreras & Silk 2000; Trager et al. 2000; Graves et al. 2009; Jeong et al. 2009), which are typically located in the quiescent part of the infrared colour-colour diagram (Temi et al. 2009).

⋆ E-mail: massimo.gaspari4@unibo.it

The problem of ISM heating and the related absence of cold gas in elliptical galaxies is long-lasting. This was investigated forty years ago by Mathews & Baker (1971) seminal paper to explain the dearth of cold ISM in typical ellipticals. They proposed that type Ia supernovae (SNIa) explosions heat and eject the ISM, which is continuously supplied by stellar winds from evolving stars. Subsequent investigations (MacDonald & Bailey 1981; Mathews & Loewenstein 1986; Loewenstein & Mathews 1987; Ciotti et al. 1991; David et al. 1991) have analysed in depth the secular evolution of the ISM in isolated ellipticals. SNIa heating is indeed able to prevent gas cooling and drive global winds in small or intermediate ellipticals but not in massive galaxies, which usually reside at the centre of a massive dark halo. These systems necessitate a different energy source.

Furthermore, galaxy formation theory requires a mechanism to halt star formation in massive galaxies in order to agree with the observed sharp cut-off of the luminosity function at the high-mass end (Benson et al. 2003; Balogh et al. 2006; Croton et al. 2006; Cattaneo et al. 2009). It is now clear that supernova heating alone is insufficient to prevent the gas from cooling and forming stars (e.g. Tornatore et al. 2003; Piontek & Steinmetz 2011). Thus, the black hole at the centre of massive galaxies becomes the natural suspect for providing the required feedback heating (Binney & Tabor 1995).

From an energetic point of view, AGNs are able to satisfy galaxies or clusters heating demand. For a typical black hole mass of $M_{\rm BH} \approx 10^9\ M_\odot$ (e.g. Ferrarese & Merritt 2000; Gebhardt et al. 2000[1]), an amount of energy $E_{\rm BH} \approx 0.1\, M_{\rm BH} c^2 \approx 2 \times 10^{62}$ erg could in principle be injected in the surrounding gas. This is a sizeable fraction of the whole energy radiated away by the intracluster medium (ICM) in a massive cluster lifetime, and is significantly larger than the binding energy of the interstellar medium in a typical elliptical galaxy or group. For example, the gas binding energy for the massive, X-ray bright group NGC 5044 is $\approx 9 \times 10^{61}$ erg (Mathews et al. 2005).

Many fundamental questions about the physics of the AGN feedback, however, remain unanswered (see also Ostriker et al. 2010). A key issue is to identify the physical process through which the AGN interact with the surrounding gas. Several mechanisms have been proposed and numerically investigated, including radiative heating by quasars (Ciotti & Ostriker 1997), cavities generated through the injection of thermal energy or cosmic rays (Dalla Vecchia et al. 2004; Brüggen et al. 2005; Mathews & Brighenti 2008; Mathews 2009; Guo & Mathews 2010), or bipolar mechanical outflows/jets (Omma et al. 2004; Soker & Pizzolato 2005; Zanni et al. 2005; Brighenti & Mathews 2006; Vernaleo & Reynolds 2006; Brüggen et al. 2007; Gaspari et al. 2009, 2011a,b, 2012).

In low-redshift systems it seems likely that massive black holes mostly accrete mass and return energy in a radiatively inefficient way (Fabian & Rees 1995; Loewenstein et al. 2001; Di Matteo et al. 2003; Taylor et al. 2006). Thus, while luminous quasars might have been an important source of heating at high redshift, with the peak of the QSO distribution at $z \sim 2$, (Nesvadba et al. 2008; Moe et al. 2009; Dunn et al. 2010a), observations point to advection dominated accretion flow (ADAF)-like systems as a primary source of local AGN feedback. These accretors naturally generate powerful outflows (Narayan & McClintock 2008 and references therein).

Recent X-ray and radio observations (see the reviews by McNamara & Nulsen 2007 and Gitti et al. 2012) provide a crucial guidance to narrow down the range of the possible heating scenarios. The common presence of radio-filled X-ray cavities, ellipsoidal weak shocks and metal (iron) enhancements along the radio jet path (e.g. Gitti et al. 2010; Kirkpatrick et al. 2011; Randall et al. 2011) strongly suggests that local AGNs introduce energy directionally and in mechanical form, likely as bipolar massive outflows or jets.

For this reason in Gaspari et al. (2011a,b – G11a,b) we tested a variety of outflow models in clusters and groups in order to verify if this mechanical feedback is able to quench cooling without overheating the core, an often unwelcome byproduct of central energy injection (Brighenti & Mathews 2002, 2003, 2006). We showed that massive, subrelativistic outflows are indeed a viable mechanism to solve the cooling flow problem in clusters and groups. In lighter systems the AGN feedback must be however more gentle and continuous, or, in other words, in massive clusters a possible quasi continuous low-power activity must be intermixed with sporadic powerful events.

In the present work we study how the AGN feedback self-regulates in a galactic environment and test the models against several observational constraints. Massive elliptical galaxies are in fact important laboratories to study the AGN feedback process in the local universe. Their ISM shines in X-ray and many giant ellipticals are relatively nearby, within a distance of $\sim 15 - 30$ Mpc – a valuable virtue compared to X-ray bright, but distant, massive clusters. The relative proximity allows thus the investigation of a region closer to the AGN, where the feedback engine might manifest itself in a clearer way.

In Section 2 we present our theoretical modelling and the details of the numerical methods. We adopt a simple recipe to activate the outflows, based on gas cooling near the central black hole. We discuss in Sec. 2.1.1 why it is not feasible to investigate with appropriate accuracy the accretion and the outflow generation processes. We turn instead our attention to the effect of the outflows on large scales. We analyse the observable consequences of the assumed feedback scenario on the environment of an isolated elliptical (Section 3) and a galaxy with circumgalactic gas (Section 4). In Section 5 and 6 we discuss the key features of the results presented in this work and summarise the effects of mechanical AGN feedback on every scale, from galaxies to massive clusters.

2 THEORETICAL AND NUMERICAL SETUP

2.1 AGN feedback

2.1.1 What is the accretion rate?

As remarked in the Introduction, massive black holes in nearby X-ray bright ellipticals likely accrete gas through a

[1] The most massive BH at the centre of brightest clusters can be even an order of magnitude heavier, like the BH in NCG 4889 with $M_{\rm BH} \sim 2 \times 10^{10}\ M_\odot$ (McConnell et al. 2011).

radiatively inefficient mechanism. ADAF models naturally predict outflows and jets (Narayan & McClintock 2008), which might provide the mechanical feedback we study in the present article.

Our feedback scheme assumes that the black hole reaction is proportional to the accretion rate (Sec. 2.1.2). This simple conjecture leads, however, to a substantial difficulty in building a self-consistent model, i.e. properly estimating the BH accretion rate. This is such a complex problem that we should not be ashamed to accept our ignorance. We give below some reasons why the accretion rate (and the BH growth) can not be investigated in depth within the frame of our models, and must therefore be estimated with some subgrid scheme, which usually depends on the uncertain gas properties in the nuclear region. Because the simulated ISM in the central few hundreds pc is quite different from that of real ellipticals, our calculated accretion rate should not be trusted with high confidence. We suspect that this is true for most numerical works on AGN feedback, either in galaxies or clusters. Specifically, the motivations which lead to a rather uncertain accretion rate are the following.

(i) In order to self-consistently model the three-dimensional accretion flow, using magneto-hydrodynamics, the necessary condition is to numerically resolve a region with size a few Schwarzschild radii, $R_{\rm S} \approx 3 \times 10^{14} (M/10^9 M_\odot)$ cm $\approx 10^{-5} R_{\rm B}$ (where $R_{\rm B}$ is the usual Bondi radius). This is currently not feasible for (3D) simulations aimed to investigate galactic-scale flows. Because the direct calculation is impractical, we are left to rely on a subgrid prescription to estimate the accretion rate. However, this is a formidable task; the exact quantitative of material that is considered 'accreted' must be taken with serious caution and only as a rough approximation.

(ii) Many studies – including ours (G11a,b) – use the Bondi (1952) theory to estimate the instantaneous mass accretion rate onto the BH (e.g. Springel et al. 2005; Cattaneo & Teyssier 2007; Sijacki et al. 2007; Puchwein et al. 2008; Booth & Schaye 2009; Dubois et al. 2010). In order to make results compatible with observations, the Bondi accretion rate is often artificially and arbitrarily boosted by a factor of ~ 100 (see Booth & Schaye 2009 for a related discussion). While this is a convenient parametrisation, it seems unsafe to rely on it for a realistic representation of the accretion process. Beside complications such as turbulence, rotation and magnetic fields (see Krumholz et al. 2005, 2006; Igumenshchev 2006; Mościbrodzka & Proga 2008, 2009; Narayan & Fabian 2011), which can easily change the classic accretion rate by a factor of a few, we believe that cooling (and heating) make the Bondi assumption particularly hazardous. The central ISM can be prone to thermal instabilities which can drastically change the nature of the accretion process (Pizzolato & Soker 2005; Gaspari et al. 2012; McCourt et al. 2012; Sharma et al. 2012). In fact, in the presence of a classical cooling flow the mass inflow rate at some small radius is determined by the gas cooling process rather than the BH gravity. Thus, we expect $\dot{M}_{\rm BH} \approx 0.1 - 1$ M$_\odot$ yr^{-1} for an isolated elliptical galaxy. Accretion scenarios suggested by King & Pringle (2007) and Pope (2007, 2009) also differ significantly from the Bondi prediction.

The common assumption in numerical models is to take as Bondi boundary conditions some average of density and temperature within a radius larger than $R_{\rm B}$, usually a simulated region filled with smooth hot gas. However, the real ISM at the fiducial Bondi radius for the hot gas (≈ 50 pc) is often constituted by a multiphase, dusty $\sim 10^4$ K gas (Heckman et al. 1989; Shields 1991; Buson et al. 1993; Goudfrooij et al. 1994; Macchetto et al. 1996; Ferrari et al. 1999; Martel et al. 2000; Tran et al. 2001; Colbert et al. 2001; Verdoes Kleijn et al. 2002), which can be both dynamically relaxed or in chaotic motion (Caon et al. 2000; Sarzi et al. 2006, 2010). This warm gas is likely intermixed with hot ISM, and the interaction between the two phases is poorly understood. With such a complex gas conditions it is difficult to estimate the accretion rate. With 1D or 2D simulations it is relatively easy to resolve the Bondi radius in galactic flows (e.g. Ciotti & Ostriker 1997; Brighenti & Mathews 1999; Quataert & Narayan 2000; Novak et al. 2011), yet the necessarily simplified gas physics adopted and the limits imposed by the geometry prevent these models to catch the complexity of the ISM near the black hole.

Because of these (not easily quantifiable) uncertainties we prefer to not assume any sophisticated subgrid modelling for the accretion process.

(iii) Finally, the assumptions made for stellar source terms (smooth injection of mass and energy from evolved stars and SNIa), described in Section 2.2.1 (see also Mathews & Baker 1971; Loewenstein & Mathews 1987; Mathews & Brighenti 2003), clearly break down within the galactic core. A mature SNIa remnant would have a size of ≈ 50 pc if the external medium has a number density of ~ 0.1 cm^{-1} and a temperature $\sim 10^7$ K, comparable with the galactic core radius. Stellar winds from orbiting stars likely generate long tails of warm gas, several tens of pc in size (Mathews 1990; Parriott & Bregman 2008; Bregman & Parriott 2009), giving rise to inhomogeneities. The stellar material can indeed help explaining the ubiquitous presence of emission line gas at the centre of early-type galaxies (Mathews & Brighenti 2003). These intrinsic limitations, along with the lack of merging as possible source of gas, hamper a proper modelling of the ISM in the central $\approx 100 - 200$ pc.

For all the previous reasons, we believe that it is futile to investigate the details of BH accretion history in the present work. Therefore, we realistically limit the goal of our study to the effects of (large scale) outflows on the ISM evolution.

2.1.2 Self-regulated mechanical outflows

Encouraged by the results in G11a and G11b for clusters and groups, we consider here subrelativistic collimated outflows as the main ingredient of the AGN mechanical feedback in elliptical galaxies. In considering massive slow outflows, we are implicitly assuming that the relativistic jet entrains some ISM mass (the active mass $M_{\rm act}$, defined below) or perhaps that a wind originate from the accretion disk (e.g. Crenshaw et al. 2003; Morganti et al. 2007; Nesvadba et al. 2008; Cappi et al. 2009, 2011; Tombesi et al. 2010a,b, 2012; see also the references in G11a,b). Moreover, radio jets are highly relativistic on pc scale, but rapidly decrease to subrelativistic velocities within few kpc from the black hole (Giovannini 2004).

In G11b we showed that, on galaxy group scales, the self-regulation imposed by cold gas accretion tends to gen-

erate a quasi-continuous, gentle feedback, qualitatively similar to what expected for a boosted (by a factor of ~ 100) Bondi accretion. However, on top of this low level AGN activity, several powerful outbursts can occur, which produce visible cavities and shocks, a desirable feature of those models. Therefore, in the present work on elliptical galaxies, we preferred to adopt a cold feedback mechanism (see also Pizzolato & Soker 2005), where the assumed accretion rate is linked to the cooled gas in a given central region. As pointed out in Section 2.1.1, there are several reasons to believe that a purely Bondi accretion scenario (that is, the hot feedback mode) is inappropriate.

We slightly improved the feedback self-regulation mechanism compared to G11a,b. The radius of the region used to estimate the accreted cold gas – usually several kpc – was of course rather arbitrary, and we assumed that the jet is instantaneously triggered only by the gas cooled near the centre of the system. This lengthscale was reasonable because almost all the cooling occurred inside the chosen radius.

In order to eliminate this parameter, we adopt here the physical assumption that the cooled gas (dropped out at radius $r_{\rm i}$) goes into free fall and accretes onto the black hole in a free-fall time, given by

$$t_{\rm ff} = \int_{r_{\rm i}}^{0} \frac{dr}{\sqrt{2\,|\phi(r) - \phi(r_{\rm i})|}}\,, \qquad (1)$$

where ϕ is the gravitational potential (associated with the stellar and dark matter mass distribution). We also impose that the infalling gas must have a low angular momentum, i.e. less than $v_{\rm c}(\Delta r)\,\Delta r$ (circular velocity times the minimum radial grid size). Most of the cooled gas has nevertheless a negligible angular momentum.

The cold mass reaching the centre at a given time, $\Delta M_{\rm c,tot}$, triggers an outflow with kinetic energy given by

$$\Delta E_{\rm jet} = \epsilon\,\Delta M_{\rm c,tot}\,c^2, \qquad (2)$$

where ϵ is the parametrized mechanical efficiency of the feedback. It is likely that the efficiency depends on the ratio between the actual accretion rate and the Eddington rate, $\dot{M}_{\rm Edd} \approx 22\,(M_{\rm BH}/10^9 M_\odot)\ M_\odot\,{\rm yr}^{-1}$ (Churazov et al. 2005; Merloni & Heinz 2008). However, given the uncertainties in estimating the accretion rate, we prefer to assume a constant efficiency.

This kinetic energy (and the associated momentum) is given to the hot gas located in a small region at the centre of the grid (the 'active' jet region), whose size is usually[2] $\Delta R \times \Delta z = 2 \times 1$ cells (about 300 pc wide, 150 pc high), containing some hot gas mass $M_{\rm act}$. The outflow velocity was retrieved as usual (G11a,b), imposing

$$\frac{1}{2} M_{\rm act} v_{\rm jet}^2 = \Delta E_{\rm jet}. \qquad (3)$$

[2] A slightly smaller or larger active region does not drastically alter the global evolution (see G11a,b). The same is true if we inject the energy from the internal boundaries of the grid.

2.2 Galaxy models

2.2.1 Isolated elliptical

In this Section we describe the modelling of the elliptical galaxy, providing the initial conditions for the simulations. We model the massive elliptical galaxy with a de Vaucouleurs' stellar density profile (approximated as in Mellier & Mathez 1987), with effective radius $r_{\rm eff} = 8.5$ kpc and total stellar mass $M_* = 7 \times 10^{11}\ M_\odot$. Assuming a stellar mass-to-light ratio of 8 (in the B band), appropriate for an old stellar population, the resulting luminosity is $L_B = 8.75 \times 10^{10}\ L_\odot$. Thus, our model represents a typical elliptical galaxy similar to NGC 4649, NGC 4472 and many others in the local universe, albeit without the intragroup medium. The dark matter is modelled as a NFW halo (Navarro et al. 1996) with virial mass $M_{\rm vir} = 4 \times 10^{13}\ M_\odot$ and a concentration $c = 8.8$ (Bullock et al. 2001; Humphrey et al. 2006).

Several ingredients characterise the stellar mass and energy sources (stellar winds and SNIa). The specific stellar wind mass return rate is assumed to be $\alpha_* = 4.7 \times 10^{-20} (t/t_{\rm n})^{-1.3}\ {\rm s}^{-1}$, where $t_{\rm n} = 13$ Gyr is the galaxy age (results are not sensitive to the adopted $t_{\rm n}$). This formula is a good approximation for a single stellar population older than 100 Myr. The SNIa mass return rate depends on the SNIa rate, $r_{\rm Ia} = 0.06\,(t/t_n)^{-1.1}$ SNu (Cappellaro et al. 1999; Greggio 2005; Mannucci et al. 2005). With the chosen SNIa rate, the specific SNIa mass return rate is $\alpha_{\rm Ia} = 3.17 \times 10^{-20}\, r_{\rm Ia}(t)(M_{\rm ej}/M_\odot)/(M_*/L_B)$, where $M_{\rm ej} = 1.4\ M_\odot$ is the ejecta mass of a SNIa and $M_*/L_B = 8$ is the stellar mass-to-light ratio in the B band. The adopted $r_{\rm Ia}$ results in gas abundances consistent with observations (Humphrey & Buote 2006).

The energy injection associated to stellar winds and SNIa is treated as outlined in Mathews & Brighenti (2003). The stellar velocity dispersion, which determines the temperature of the injected wind gas, is calculated by solving the Jeans equation for a spherically symmetric, isotropic stellar system. Fortunately, the stellar wind heating has not a large impact on the flow and it is not necessary to calculate $\sigma_*(r)$ using more sophisticated dynamical models.

Concerning the gaseous component, we decided to simulate two kinds of systems. In the first one, indicated as the 'isolated galaxy', the ISM is produced by internal processes alone (stellar mass loss and SNIa ejecta). Although the hot ISM of massive, X-ray bright ellipticals can not be realistically explained without a circumgalactic gas component (Brighenti & Mathews 1998; Brighenti & Mathews 1999), we decided to use this approach for its simplicity and to allow a direct comparison with previous calculations of hot gas flows in ellipticals (e.g. Loewenstein & Mathews 1987; Ciotti et al. 1991; Ciotti & Ostriker 1997). Within $\sim r_{\rm eff}$ most of the ISM is indeed likely to come from stellar mass loss (Brighenti & Mathews 1999). Thus, the terminology 'isolated galaxy' does not refer to the presence of other (large) galaxies nearby, but that the ISM is not contaminated by the group or cluster gas.

The simulations of the isolated galaxy start at cosmic time $t = 1$ Gyr with the galaxy essentially devoid of gas, conforming to the usual assumption that the gas has been cleared by a SNII-driven wind. The ISM is then gradually supplied by the stars. After few 10^8 yr, the system loses memory of the initial conditions and, if not heated,

approaches a quasi-steady state, with secular changes controlled by the slow variation of the stellar mass return rate (Loewenstein & Mathews 1987; Ciotti et al. 1991). The simulations are evolved to final time, 13 Gyr.

2.2.2 Elliptical with circumgalactic gas

In the second class of models, more realistic and appropriated for a detailed comparison with well-observed galaxies, we take into account the presence of the circumgalactic gas (CGG). Many of the famous X-ray ellipticals belong to this breed. A distinctive characteristic of classic cooling flow models with CGG is the presence, often observed in real systems, of a relatively broad cool core, in perfect analogy with galaxy clusters (Brighenti & Mathews 1998; Brighenti & Mathews 1999; Humphrey et al. 2006; Diehl & Statler 2008b). The separation between galaxies with CGG and galaxy groups is largely semantic, so these models are tightly linked to those calculated in G11b. However, here we focus mainly on the region close to the galaxy ($r \lesssim r_{\rm eff}$). At variance with G11b, we used an improved feedback scheme (Sec. 2.1.2) and adopted a significantly higher numerical resolution.

The galaxy parameters are chosen to agree with NGC 5044, a X-ray bright galaxy in the centre of the homonymous group, with $r_{\rm eff} = 10$ kpc, $M_* = 3.4 \times 10^{11}\ M_\odot$ and $M_*/L_B = 7.5$ (see Buote et al. 2004). In these simulations we use the observed $T(r)$ and $n(r)$ profiles (David et al. 1994; Buote et al. 2003; dotted lines in Figure 4) to retrieve the total gravitational potential under the assumption of hydrostatic equilibrium.

We run the CGG models for 7 Gyr. As emphasised in G11a, it is crucial to check the long-term behaviour of a heated model in order to assess its merit. Unfortunately, short-term simulations can in fact return misleading results on a particular feedback model as a solution of the cooling flow problem.

2.3 Numerical techniques

2.3.1 Code setup

As in G11a,b we have used a substantially modified version of the 3D hydrodynamic code FLASH 3.3 (Fryxell et al. 2000). The main advantages include the adaptive mesh refinement (AMR) block structure, suited for a very efficient scalability trough the Message-Passing Interface (MPI). The simulations were carried out on the parallel high-performance clusters SP6 (CINECA) and Pleiades (NASA). We employed the PPM split scheme to treat the transport terms in the conservation equations (in principle third-order accurate). A full description of the hydrodynamic equations can be found in G11a,b, with the additional source terms representing AGN feedback, radiative cooling, and stellar winds plus SNIa.

The computational rectangular 3D box in almost every model extends up to 150 kpc. We have simulated the $z > 0$ half-space with reflection boundary condition at $z = 0$, setting elsewhere the usual outflow condition with inflow prohibited. Despite the AMR capability of FLASH, we have decided to use a number of concentric fixed grids in cartesian coordinates. This ensures a proper resolution of the waves and cavities generated in the core by the AGN outflows. We employed a set of 7 grid levels (basic blocks of $16 \times 16 \times 8$ points), with the zone linear size doubling among adjacent levels. The most distant regions from the centre are covered by at least level 4. The finest, inner grid (level 7) has a resolution of $\Delta x = \Delta y = \Delta z = 146$ pc for the isolated galaxy models, and covers a spherical region of ~ 8 kpc in radius. For the simulations with circumgalactic gas we were forced to lower the resolution to save computational time, $\Delta x = 293$ pc (the inner grid covers $r \sim 16$ kpc); the box is instead four times bigger (8 levels). In general, grids of every level extend radially for about 55 cells. This is arguably the best way to cover very large spatial scales (hundreds pc up to hundreds kpc) and at the same time integrating the system for several Gyr.

2.3.2 Radiative cooling

The radiative cooling is a necessary ingredient for studying the cooling flow problem. We adopt the cooling function by Sutherland & Dopita (1993), dependent on gas temperature and metallicity, $\Lambda(T, Z)$, for a fully ionised plasma. The iron abundance is consistently calculated by solving a passive advection equation for the iron density, with the appropriate sources representing the injection of metals by stellar winds and SNIa (Mathews & Brighenti 2003). We assume that the abundance of all heavy elements in solar units is the same as the iron one. Although this is not strictly true, it has a negligible effect on the cooling process.

We numerically handle the gas cooling at very low temperatures by using a dropout (mass sink) term: $-q(T)\rho/t_{\rm cool}$. This is a convenient scheme to remove cold gas from the numerical grid without altering the calculated cooling rate (see G11a for more details).

The numerical implementation has been improved. As commonly done, we are using the splitting method for adding the source/sink terms, i.e. first solving the standard hydro-equations and then, adopting the updated flow variables, integrating the ordinary differential equation (ODE) associated with the source term. The ODE related to cooling is solved through a second-order Runge-Kutta explicit method. Expanding the cooling time, $t_{\rm cool} = 2.5\, n k_{\rm b} T / n_{\rm e} n_{\rm i} \Lambda(T, Z)$, and centring the variables, leads to the the following discretisation for the dropout ODE:

$$\rho^{\rm n+1} = \rho^{\rm n} \left(1 + \frac{\mu}{2.5\, k_{\rm b} \mu_{\rm e} \mu_{\rm i} m_{\rm p}} \frac{q^{\,\rm n+1/2}\, \Lambda^{\rm n+1/2} \rho^{\rm n}}{T^{\,\rm n+1/2}}\, \Delta t \right)^{-1}, \quad (4)$$

where the indexes refer to the temporal states, Δt is the timestep, and the molecular weight per particle, electron and ion are $\mu \sim 0.62$, $\mu_e \sim 1.18$ and $\mu_i \sim 1.30$, respectively; $T^{n+1/2}$ is conveniently provided by the previous Runge-Kutta midpoint estimate. The functional form of $q = 2 \exp[-(T/T_{\rm c})^2]$ ensures that the gas is considered cold and dropped out of the flow as soon as it approaches $T_{\rm c}$. Setting $T_{\rm c} = 2 \times 10^4 K$ prevents the formation of very cold clumps in the flow, whose physical evolution can not be easily followed by the present computations. It has also the benefit to prevent the drastic decreasing of the timestep. Lowering $T_{\rm c}$ permits to follow better the formation of local thermal instabilities, nevertheless the global evolution of the

Table 1. Properties of the most relevant simulations.

Model	Feedback	efficiency (ϵ)	Notes
iso-CF	no AGN heating	-	isolated
cgg-CF	no AGN heating	-	CGG
iso-1em4	cold	10^{-4}	isolated
iso-3em4	cold	3.3×10^{-4}	isolated
iso-1em3	cold	10^{-3}	isolated
cgg-8em4	cold	8×10^{-4}	CGG

cold gas and associated feedback is essentially the same on long timescales (see Gaspari et al. 2012).

The dropout term, as any source step, has a time limiter condition associated. Using the dropout ODE equation, we find that the relative density decrement, $D = 1-\rho^{n+1}/\rho^{n}$, is linked to the following timescale: $t_{\rm drop} = [D/q(1-D)]\, t_{\rm cool}$. It is evident that the dropout limiter is tightly correlated with the cooling limiter, $\eta\, t_{\rm cool}$ (with $\eta < 1$). Limiting the variation of internal energy has the consequence to directly reduce the dropped mass, quantitatively: $D = \eta\, q/(1+\eta\, q)$. In order to smoothly couple the hydro-solver to the sink terms, a reasonable limiter is $\eta = 0.4$; since the maximum q value can be 2, the dropout decrement will never exceed $\approx 45\%$ per timestep (it is usually much lower).

3 RESULTS: ISOLATED GALAXY

In Section 3 we report the results for models in which the ISM is produced only by the mass loss of the galactic stellar population. We explore the effect of the mechanical feedback varying the key parameter, the efficiency ϵ (see Table 1). In order to solve the cooling flow problem, AGN outflows must quench the cooling flow, without overheating the ISM in a drastic way. The former request is easy to satisfy, if the feedback is energetic enough. The simultaneous fulfilment of the two conditions above is instead complicated, and often require an unpleasant fine tuning of the heating parameters (Brighenti & Mathews 2002, 2003). A successful feedback needs also to reproduce other observational features, such as cavities, shocks, turbulence, multiphase gas, and metals dredge-up.

3.1 Pure cooling flow

In Figure 1 we show the relevant global quantities which characterise a pure cooling flow model, with AGN heating switched off and the heating provided mainly by the SNIa. This is a classic result: the densest gas loses thermal pressure support due to radiative losses, inducing a slow subsonic inflow ($v_{\rm r} \lesssim 50$ km s^{-1}) that further increases the plasma emissivity (a detailed discussion can be found in Mathews & Brighenti 2003 and references therein). We emphasise that when no AGN heating is considered, the gas cooling rate (top panel), occurring at the very centre of the galaxy, roughly decreases in pace with the stellar mass loss ($\dot{M}_* \propto t^{-1.3}$), reaching $\dot{M}_{\rm cool} \approx 1\ M_\odot$ yr^{-1} at $t = 12.7$ Gyr, when the simulation ends. Needless to say, this is a much larger cooling rate than allowed by the observations quoted in the Introduction.

The X-ray luminosity also secularly drops, from $L_{\rm X} \sim 5 \times 10^{42}$ erg s^{-1} at $t = 2$ Gyr to $\sim 9 \times 10^{41}$ erg s^{-1} at final time. We refer here to the bolometric X-ray luminosity, calculated within $r \lesssim 200$ kpc. The reason for the luminosity drop is the decline of the ISM density illustrated in the middle panel of Figure 1. The slope of the density radial profile does not vary significantly with time and, as expected, is too steep at the centre, a well known problem of classical cooling flow models (Sarazin & White 1988; Sarazin & Ashe 1989).

We also note that classical cooling flows in isolated galaxies lack the large cool core typical of cooling flow clus-

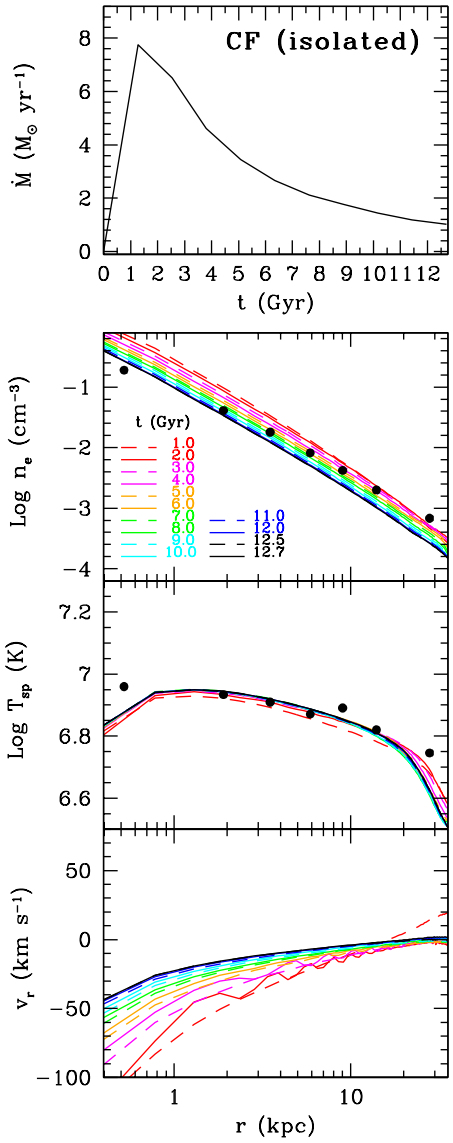

Figure 1. Evolution of the cooling flow model (no AGN feedback), for the isolated galaxy (iso-CF). From top to bottom panel: gas cooling rate ($\dot{M}$) as a function of time, radial profiles of electron number density ($n_{\rm e}$), projected spectroscopic-like temperature ($T_{\rm sp}$), and radial velocity ($v_{\rm r}$). Times and colours are indicated in the second panel. Filled circles represent observational data points for the elliptical galaxy NGC 6482 (Khosroshahi et al. 2004; Diehl & Statler 2008b). See Section 3.1 for more details.

ters or groups (see the spectroscopic-like[3] temperature profile in the third panel). Instead, the temperature monotonically increases toward the centre (except for the very inner region). This can be understood because the steep gravitational potential associated with the peaked de Vaucouleurs' density profile (the dark halo is sub-dominant within $r_{\rm eff}$) provides enough gravitational heating to the inflowing – thus compressing – gas to balance the radiative losses; needless to say, this process terminates when the gas reaches the centre, where it cools catastrophically.

Ideally, we would compare the profiles with a well-observed elliptical which is at the same time massive *and* isolated, in the sense of Section 2.2.1. However, most of the known giant ellipticals reside at the centre of groups or clusters and their hot ISM is contaminated by the CGG. NGC 6482 is one of the few massive and X-ray bright ellipticals with a negative temperature gradient (Khosroshahi et al. 2004) and we show the data of this system in Figure 1 for comparison. On the other hand, we note that NGC 6482 presents some differences compared to our model. The dark halo is less massive (Khosroshahi et al. 2004; Humphrey et al. 2006) and it owns a relatively extended X-ray halo with $L_{\rm X} \sim 10^{42}$ erg s^{-1}, likely contaminated by CGG. Nevertheless for $r \lesssim r_{\rm eff}$, i.e. the region more relevant to our investigation, the hot gas should be dominated by the internal component only.

3.2 AGN feedback: $\epsilon = 10^{-4}$

We now describe some results for the simulations with AGN feedback, progressively increasing the efficiency and focusing on their global properties. We compare them with the cooling flow model discussed above and perform a critical analysis of the observable quantities. The first three rows of Figure 2 show the gas cooling rate, plus the radial profiles of electron number density and (projected) spectroscopic-like temperature, for three representative feedback models.

In the first column, top panel, the model with $\epsilon = 10^{-4}$ exhibits a cooling rate significantly reduced with respect to the iso-CF simulation (red vs. black line), with an average value of $\sim 0.4\ M_\odot$ yr^{-1} and $\dot{M}(12.7\,{\rm Gyr}) \sim 0.2\ M_\odot$ yr^{-1}. These numbers are probably still too high compared to available X-ray and UV observations (Bregman et al. 2001, 2005; Xu et al. 2002; Tamura et al. 2003) or star formation estimates in massive ellipticals (Temi et al. 2009).

The density profile (second panel) oscillates in time, especially in the inner region, but retains reasonable values, as can be noticed through a comparison with typical observations of ellipticals (Humphrey et al. 2006).

The density cycles correspond to the accumulation of gas during periods of less intense AGN activity, e.g. between 6 and 7 Gyr there is no powerful outburst. This leads to an increase of the gas density in the central region, a higher cooling rate and finally a powerful ($\sim 3\times10^{44}$ erg s^{-1}) event which quickly expands the hot gas atmosphere. The density cycles also reflect in the variation of the X-ray luminosity which, in turn, fluctuates between $10^{41} \lesssim L_{\rm X} \lesssim 2\times10^{42}$ erg s^{-1} (with a mean value of $\sim 10^{42}$ erg s^{-1}). This variation can in part explain the long-standing problem of the scatter in the L_B (or L_K) - $L_{\rm X}$ diagram (Eskridge et al. 1995; Beuing et al. 1999; Ellis & O'Sullivan 2006), along with the occurrence of SNIa winds (Ciotti et al. 1991; David et al. 2006) and the variation of the dark halo masses at a given optical luminosity (Mathews et al. 2006).

The temperature profile is a sensitive probe of AGN heating scenarios, yet often neglected in the comparison with observations. As expected, heating processes originating close to the galactic core often overheat the central ISM, an effect rarely or never observed in real galaxies (Brighenti & Mathews 2002, 2003). The best observed systems (which, unsurprisingly, are the X-ray brightest) commonly show positive temperature gradient, with the centre hosting the coolest X-ray gas of the system (Humphrey & Buote 2006; Diehl & Statler 2008b). On the other hand, observed galaxies which are isolated or in a less dense environment usually show a moderate negative or flat T gradient.

In the third panel (left column) we show the radial profile of the spectroscopic-like temperature at twelve different times. In this feedback model the ISM is never overheated in the central region and always maintains an acceptable thermal structure (Kim & Fabbiano 2003; Fukazawa et al. 2006; Humphrey et al. 2006; Sansom et al. 2006; Diehl & Statler 2008b; Nagino & Matsushita 2009), i.e. the central negative T gradient is rather shallow and the central temperature remains at or below $\sim 10^7$ K. The lack of a substantial cool core must be ascribed to the absence of the CGG, not to the presence of the AGN feedback. Ripples in the temperature profile are caused by weak shock waves generated by the AGN outbursts. However, these waves would be largely diluted if the azimuthal average is made in relatively larger radial bins, as in real observations. We did not try here to exactly generate a fully synthetic observation of the simulations (see Heinz et al. 2011) and limit our analysis to spectroscopic-like, projected quantities.

The last three rows of Figure 2 show the detailed evolution of the mechanical feedback (for the single jet). The total injected energy ($E_{\rm jet}$) for this model is 3×10^{59} erg, the typical power ($P_{\rm jet}$) is on the order of $3\times10^{42} - 10^{43}$ erg s^{-1}, with velocities ($v_{\rm jet}$) around 10^4 km s^{-1}.

3.3 AGN feedback: $\epsilon = 10^{-3}$

The previous model, with efficiency $\epsilon = 10^{-4}$, was found in satisfactory agreement with several observational constraints. However, the cooling rate, although significantly reduced with respect to the classical iso-CF model, was still too large compared with observational limits. It is thus natural to increase the heating efficiency, essentially a free parameter of any current feedback scheme, to test if the cooling rate can be further reduced without scrambling the variable profiles.

When $\epsilon = 10^{-3}$ (third column in Figure 2), the effect of the feedback is excessive: the ISM becomes rarefied in the inner region ($r \lesssim r_{\rm eff}$) and simultaneously overheated. Because the $\epsilon = 10^{-3}$ model was unsatisfactory, we stopped this simulation at $t \sim 9.5$ Gyr. It is interesting that the energy released by the AGN feedback is lower when the effi-

[3] To be more adherent to observations, we avoid the idealised emission-weighted temperature, instead we use the prescription by Vikhlinin 2006 to approximately estimate a more realistic projected temperature. The two types of profile appear nevertheless similar in the majority of the cases.

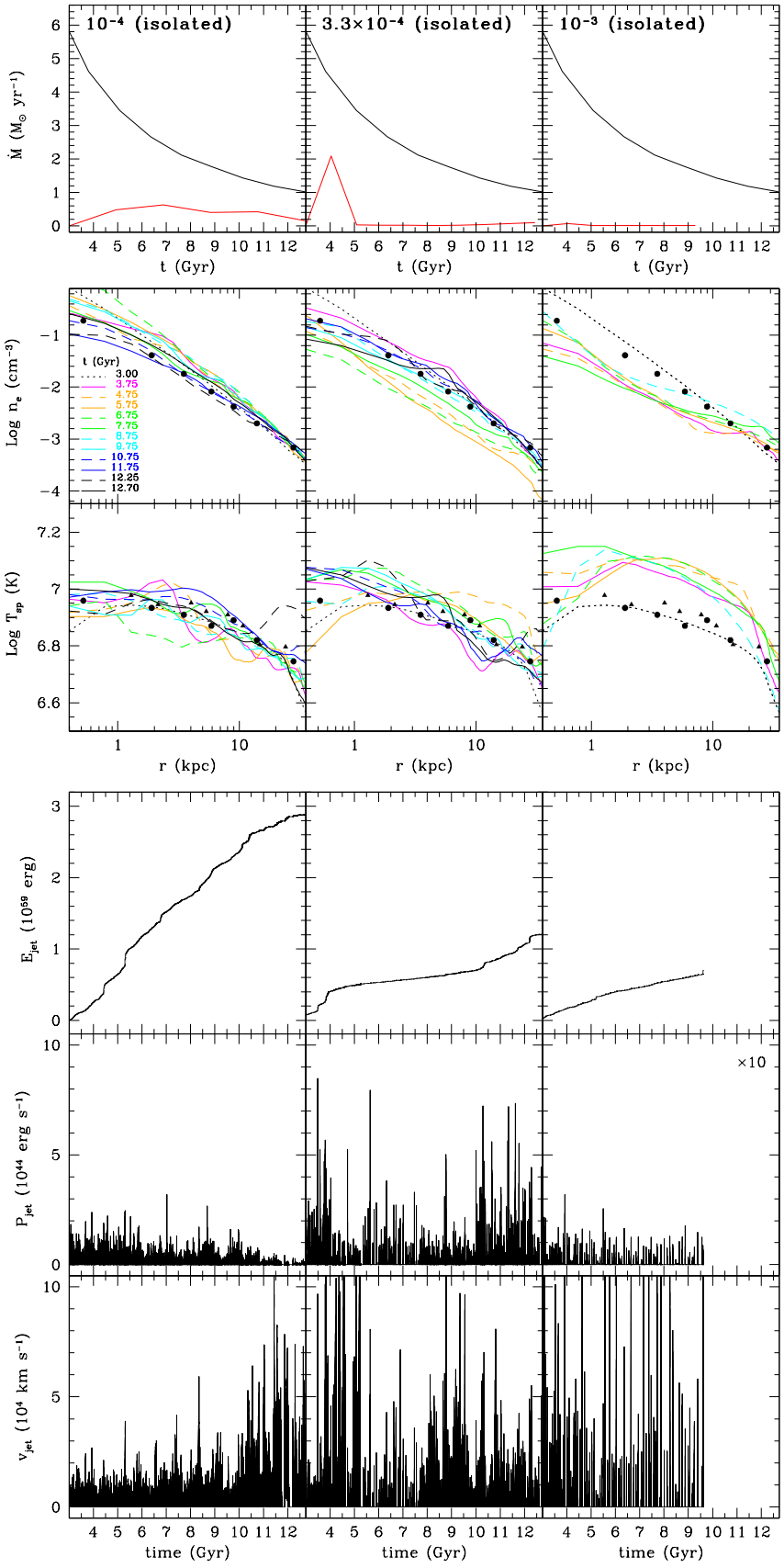

Figure 2. Evolution of the isolated galaxy with AGN feedback and increasing mechanical efficiency (from left to right column): $\epsilon = 10^{-4}$, 3.3×10^{-4}, and 10^{-3}. First three rows: gas cooling rate versus time, radial profiles of electron number density and spectroscopic-like temperature (at twelve different times). Last three rows: injected mechanical energy, instantaneous power and velocity of the AGN feedback (for the single outflow), as a function of time.

ciency ϵ is larger (cf. the fourth row of Figure 2, $E_{\rm jet} \gtrsim 10^{59}$ erg). Evidently the more powerful and faster outflows (several 10^{44} erg s^{-1} and over 5×10^4 km s^{-1}) of iso-1em3 model are able to stop the cooling flow for a relatively long time. The interval between AGN outbursts is in fact $\sim 6\times10^7-10^8$ yr, while for $\epsilon = 10^{-4}$ the AGN activates at least one order of magnitude more frequently, with the net result of injecting less energy over the galaxy lifetime. This confirms the same trend found for galaxy clusters (G11a) and illustrate that the complexity of the problem makes reasonings based on the energetic budget alone rather inaccurate.

The lower gas density implies a generally lower X-ray luminosity, with mean $\sim 5 \times 10^{41}$ erg s^{-1}. With efficiencies $\epsilon > 10^{-3}$ (models not shown), the simulated profiles strongly depart from those of real ellipticals (like NGC 6482) and the X-ray luminosity drops to undetectable values. We note here that low-$L_{\rm X}$ early-type galaxies usually show the presence of some ISM in the central region, which has a relatively low temperature (see for example NGC 4697, Sarazin et al. 2001; NGC 1291, Irwin et al. 2002; NGC 3379, Trinchieri et al. 2008). Thus, their low X-ray luminosity may not be associated with strong AGN feedback generating a galactic wind.

3.4 AGN feedback: $\epsilon = 3.3 \times 10^{-4}$

Finally, we have calculated a model with intermediate efficiency, $\epsilon = 3.3 \times 10^{-4}$, which will serve as best model in the following discussion. As displayed in the middle column of Figure 2, the cooling rate is now below the limits placed by current observations ($\lesssim 0.1\ M_\odot$ yr^{-1}), apart a narrow, transient peak at $t \sim 4$ Gyr. The density and temperature profiles vary in time slightly more than in model iso-1em4, but remain consistent with observations (cf. NGC 6482 data points). The spatial oscillations in the (projected) temperature profiles, with maximum amplitude $\sim 20\%$, are compatible with those shown in deep *Chandra* observations (see for example fig. 10 in Randall et al. 2011).

The final injected energy is 10^{59} erg (fourth panel). Typical outburst powers are in the range several 10^{42} – few 10^{44} erg s^{-1} (fifth panel), while the velocity of the outflows (bottom panel) vary in the range[4] $10^3 - 10^5$ km s^{-1}, in good agreement with nuclear outflow and feedback observations (see Introduction). The power values correspond to instantaneous accretion rates $\dot{M}_{\rm acc} = P_{\rm jet}/(\epsilon c^2) \sim 0.1 - 10\ M_\odot$ yr^{-1}.

We consider iso-3em4 the best model because the cooling rate is in good agreement with known constraints for many Gyr, and the variable profiles always resemble those of real galaxies. Thus, this model (and to a lesser extent iso-1em4) passes the first checkpoint, a necessary condition for a viable heating mechanism. In order to further test the robustness of the model, in the next Section we analyse the detailed galaxy appearance in the X-ray band. We finally note that the value of the ϵ parameter should not be taken as the exact physical value, given the uncertainties on the simulated accretion rate (Sec. 2.1.1).

[4] The relativistic factor $\gamma \sim 1.06$ is still low enough to safely using classic hydrodynamics.

3.4.1 X-ray features

In this Section we investigate the most significant X-ray features, naturally generated by the AGN heating process, like shocks and buoyant cavities. A direct comparison with a specific real system is not possible because our models are intended to be general and not tailored on an individual object. Moreover, cavities, shocks and perturbations are intermittently created, continually changing the ISM appearance. The main aim of the analysis is to show that the proposed feedback mechanism leads to ISM perturbations similar to those observed in galaxies and groups. A feedback scenario not satisfying basic requirements, such as the formation of cavities or weak shocks, must be rejected.

We discuss below several X-ray snapshots, taken at different times, of the best model iso-3em4. In Figure 3 (panel a in the top row) we show the X-ray surface brightness map of the central region after 0.75 Gyr of feedback evolution. An outburst with energy 2.85×10^{56} occurred 8×10^6 yr before the time of the snapshot. The outflow, ejected with velocity $v_{\rm jet} \sim 5400$ km s^{-1}, generated a weak shock, now at a distance ~ 6 kpc from the centre, with a Mach number $M \approx 1.2$ (calculated from $T_{\rm sp}$, which jumps from ~ 0.5 keV in the pre-shock region to ~ 0.6 keV in the post-shock ISM). The outflow generated a small X-ray cavity centred at $z = 4.5$ kpc and ellipsoidal (prolate) shape with semiaxes 1.5 and 1 kpc. The X-ray surface brightness depression within the cavity is about 20%, a typical value for observed cavities. Relatively colder rims surround the cavity, although the $T_{\rm sp}$ difference between the rims and the nearby gas is only $\sim 10\%$ (Fig. 3, panel b). We note that the ISM adjacent to the rims has been slightly heated by the weak shock. In the spectroscopic-like temperature map are also visible (but probably not detectable with current X-ray telescopes) very weak waves, separated by $\Delta r_{\rm waves} \sim 6$ kpc, corresponding to a period of $t_{\rm waves} = \Delta r_{\rm waves}/c_s \sim 1.6 \times 10^7$ yr, roughly the typical time between significant AGN outbursts at this epoch ($t = 3.75$ Gyr). We stress that these X-ray features are faint and the ISM looks quite relaxed at this time.

The situation after 0.5 Gyr ($t = 4.25$ Gyr; panels c and d) is different. At this epoch the AGN is more active and perturbs the ISM in a remarkable way. The X-ray arms and cavity have been generated by four series of AGN outbursts of moderate power (few 10^{42} erg s^{-1}), occurred in the previous 10 Myr. The energy injected during this time interval is $\sim 1.4\times10^{57}$ erg. Panel c shows that the X-ray surface brightness map is rich of features, with two symmetric bright arms, ~ 15 kpc long. This structure is similar to that observed in NGC 4636, a massive elliptical galaxy in the outskirt of the Virgo cluster (Jones et al. 2002; Baldi et al. 2009). Thus, it might be possible that the ISM of NGC 4636 has been shaped by multiple, moderate AGN outflows. It is in fact difficult to reproduce all the observed features of NGC 4636 with a single AGN outburst (Ballone & Brighenti, in prep.).

In the spectroscopic-like temperature map showed in panel d, the X-ray bright arms are slightly hotter than the local ISM. The temperature jump is about 30% (from 0.67 keV to 0.89 KeV) corresponding to a shock Mach number of ~ 1.3.

The galaxy alternates periods of quiescence, typically lasting $50 - 100$ Myr, with moments during which the AGN is more active and, consequently, the ISM more disturbed.

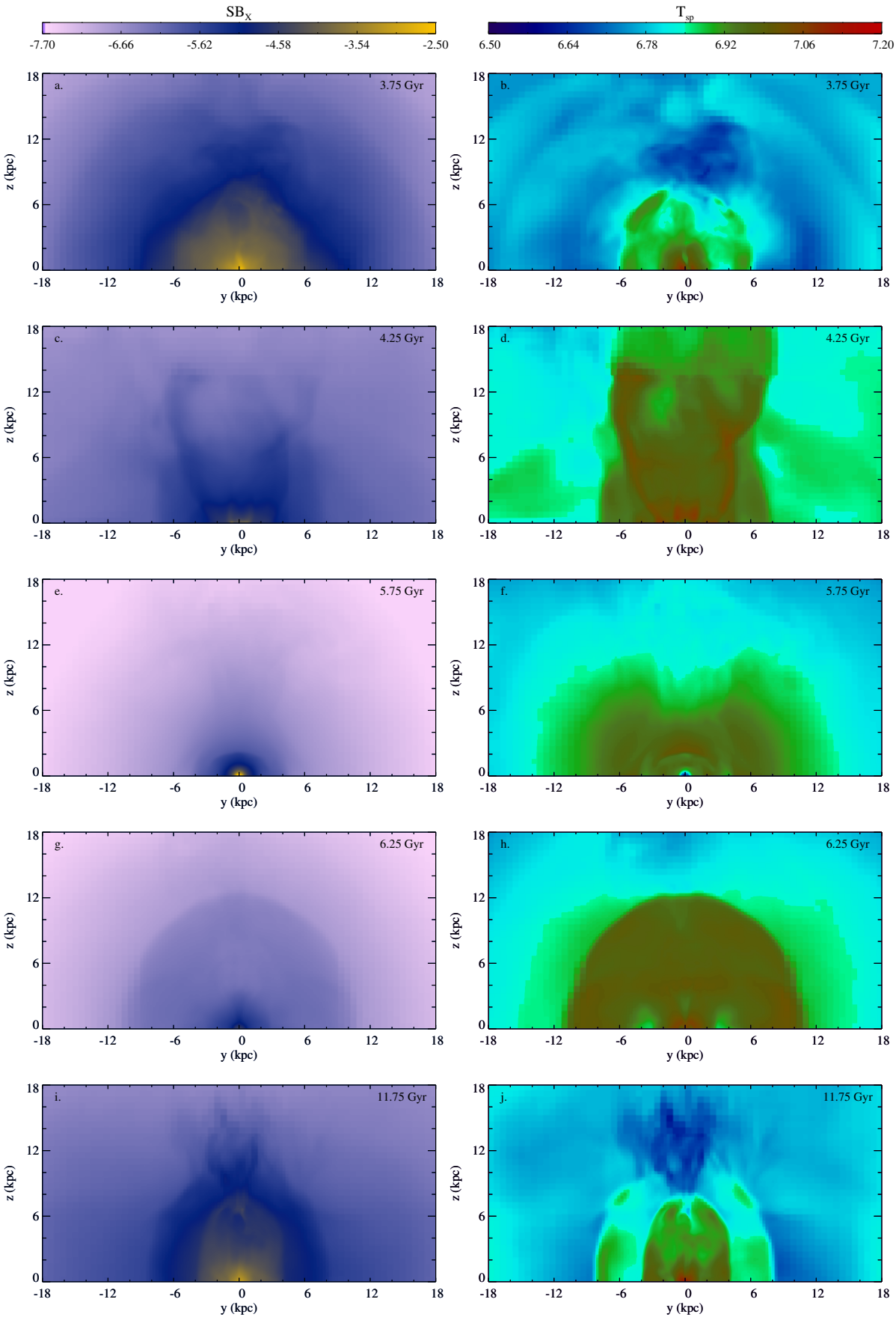

Figure 3. Maps of X-ray surface brightness (left column) and projected spectroscopic-like temperature (right column) for model iso-3em4 at five different times (from top to bottom row): 3.75, 4.25, 5.75, 6.25 and 11.75 Gyr. See Section 3.4.1.

Other interesting features appear during the evolution. At $t = 5.75$ Gyr a cold front is visible in both the brightness and temperature maps, at ~ 2 kpc from the centre (panels e and f). The front has not been caused by galaxy sloshing in our simulations, but by the encounter between gas which is falling back toward the centre, after an outflow, and the gas currently located in the central region.

At $t = 6.25$ Gyr (panel g) the brightness map shows a weak cavity about 3 kpc in radius, surrounded by a ~ 10 kpc shock with Mach number ~ 1.3 (panel h). This situation is similar to that at t=3.75 Gyr, described in panel a. This demonstrates that the ISM cyclically evolves, with recurrent cavities generated by the outflows and weak shocks, just as indicated by observations.

Although not a common circumstance, a series of shocks are visible at the same time. This occurrence is shown in panel i ($t = 11.75$ Gyr), where two ellipsoidal shocks are depicted (Mach $\sim 1.4-1.5$). The shocks intersect the $y-$axis at ~ 4 and ~ 8 kpc and are clearly visible both in the surface brightness and temperature maps (panel j).

This brief description of the ISM appearance in X-ray is intended to illustrate the richness of structures generated by the AGN outflows. Although in the present study we do not attempt a detailed comparison with real objects, it is important to realise the strong similarity of simulated features, like X-ray cavities, filaments and shocks, with the structures seen in deep X-ray observations of ellipticals and groups (e.g. Biller et al. 2004; Machacek et al. 2006, 2011; Baldi et al. 2009; Gastaldello et al. 2009; O'Sullivan et al. 2011b; Randall et al. 2011). This fact, together with the analysis in the previous Section, indicates that AGN outflows are indeed a very robust feedback mechanism, capable to highly inhibit gas cooling, keeping reasonable density and temperature profiles, and giving rise to the wealth of asymmetric structures in the ISM, seen in high-resolution deep X-ray observations.

4 RESULTS: CIRCUMGALACTIC GAS

As previously mentioned, most massive, X-ray bright ellipticals host a very extended hot ISM that can not be explained via internal processes alone (e.g. Brighenti & Mathews 1998; Brighenti & Mathews 1999). These galaxies are at the centre of large dark matter halos (Mathews et al. 2006) and the ISM is likely composed of gas shed by the stellar population, plus circumgalactic gas linked to the cosmological evolution. It is thus important to test if mechanical AGN outflows are successful for this class of objects, which include many famous X-ray targets, such as NGC 4636, NGC 4472, NGC 5044, and NGC 4649.

Interestingly, in these cool-core objects the evidence for AGN heating seems stronger, as revealed by the presence of X-ray cavities and other ISM perturbations (e.g. Biller et al. 2004; Diehl & Statler 2008a; Baldi et al. 2009; Gastaldello et al. 2009; Dong et al. 2010; Dunn et al. 2010b; Randall et al. 2011; O'Sullivan et al. 2011b). It might be a selection effect, but it is ironic (and instructive) to note that just where we know the AGN is injecting energy, the ISM close to the feedback engine is cooler than everywhere else.

4.1 AGN Feedback: $\epsilon = 8 \times 10^{-4}$

In this Section we present only the best feedback model for the CGG elliptical (efficiency $\epsilon = 8 \times 10^{-4}$), able to properly solve the cooling flow problem. It is interesting that the same feedback method requires now a larger efficiency to be acceptable, in line with the results of G11b, which indicate that in more massive systems the feedback should act more efficiently.

As in the case of the isolated galaxy, we have run a classic cooling flow model (no AGN heating) which serves as a reference calculation to gauge the effects of the feedback. We do not show the evolution of the pure CF profiles here (cgg-CF). The results are almost identical to those presented in G11b, although the numerical resolution there was about two times coarser ($\Delta x \approx 500$ pc), compared to the present model. The gas cooling rate, also indistinguishable from that in G11b, is shown in Figure 4 (black line in the top left panel). As suggested by the resulting bolometric $L_{\rm X} \sim 3 \times 10^{43}$ erg s^{-1}, the cooling rate stays around ~ 25 $M_\odot$ yr^{-1}, revealing again the cooling flow problem at the galactic/group scale.

The AGN feedback model, with $\epsilon = 8 \times 10^{-4}$ (cgg-8em4), is fully presented in Figure 4. The cooling rate (red line, first panel) has been quenched to ~ 1 $M_\odot$ yr^{-1} at the current epoch, implying a satisfactory 20-fold cooling suppression, broadly consistent with XMM-RGS observations (Tamura et al. 2003).

The spectroscopic-like temperature and density radial profiles are in excellent agreement with those observed for NGC 5044 (left column: middle and bottom panel). Remarkably, the cooling reduction did not come at the expense of the cool core: the temperature still decreases toward the galactic centre – a fundamental quality of anisotropic mechanical feedback (gradual thermalisation).

The total mechanical energy released by the AGN is $E_{\rm jet} \sim 9 \times 10^{60}$ erg (first panel in second column), which in principle would correspond to a total mass accreted on the black hole of $\sim 6 \times 10^9$ $M_\odot$, given the assumed efficiency. This accreted mass may appear substantial, but we stress again that the simulated accretion rate is quite uncertain (SMBH can nevertheless reach masses of few 10^{10} $M_\odot$). We note that the BH growth could in principle be reduced assuming that a fraction of the cooling gas does not accrete onto the BH and is ejected with the AGN outflow; increasing the efficiency would produce the same feedback power (but adding another parameter to the scheme would not provide any further physical insight).

The most relevant astrophysical result, here, is that self-regulated massive outflows are indeed capable to solve the cooling flow problem on kpc or larger scales, although the fully consistent picture – explaining the details of the BH accretion process and the formation of the outflows – needs to be clarified in future via high-resolution investigations.

The time record of the outflow power and velocity is shown in the right column in Figure 4. Powers on the order of few 10^{44} erg s^{-1} and velocity of several 10^4 km s^{-1} are again typical for the stronger events.

We conclude that massive outflows, activated when gas cooling occurs, are able to regulate the thermal evolution of the ISM, suppressing the cooling rate by a factor 20 or more and keeping the cool-core aspect of massive, X-ray bright el-

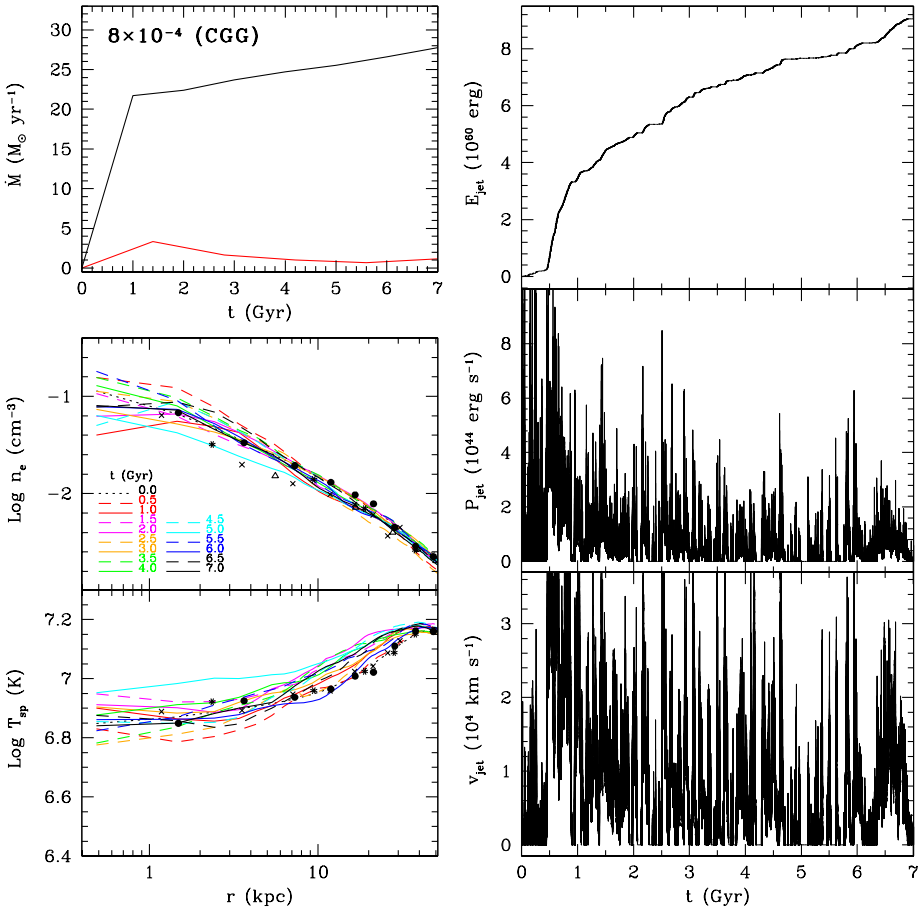

Figure 4. Evolution of the elliptical galaxy with circumgalactic gas and mechanical feedback efficiency $\epsilon = 8 \times 10^{-4}$. Left column, from top to bottom panel: cooling rate as a function of time (red line; cf. CF model – black line); electron number density and spectroscopic-like temperature at several times. The points in the last two panels represent observational data of the bright elliptical NGC 5044 (David et al. 1994; Buote et al. 2003). Right column: injected mechanical energy, (single) outflow power and velocity as a function of time.

lipticals. We now test the model via other key observational constraints.

4.1.1 X-ray features

The variety of X-ray features induced by the AGN outflows in the isolated galaxy (Sec. 3.4.1), such as buoyant bubbles and shocks, is widely present also in the CGG simulation. For the cgg-8em4 we find that the AGN activity is more frequent and powerful compared to the isolated galaxy (cf. Figures 2 and 4). Nevertheless, the X-ray appearance of the two models is remarkably similar.

In the first row of Figure 5 we show the X-ray surface brightness and spectroscopic-like projected temperature at $t = 0.5$ Gyr (panels a and b). We focus our attention on the inner 20×10 kpc of the maps, where the observations could return better details. The outflow carved a long cavity (or channel) ~ 10 kpc long and ~ 2 kpc wide. The brightness depression is about a factor of 2, which should make this feature detectable in deep, high-resolution images. For $z \lesssim 4$ kpc the cavity is surrounded by sharp bright rims (or filaments), which remind the southern open cavity in NGC 5044 (Buote et al. 2003; David et al. 2009; Gastaldello et al. 2009). The cavity is slightly hotter (by $\sim 10\%$, see $T_{\rm sp}$) than the nearby gas. At $z \gtrsim 6$ kpc broad regions ($\Delta y \sim 3$ kpc) of enhanced surface brightness, confining the X-ray feature, are present. This channel is typically fragmented by AGN turbulence or strong recurrent outbursts. On the $z = 0$ plane, close to the centre, the inflowing gas forms a dense torus which is punched, but not cleared away, by the outflows. This feature could, however, be numerically amplified by the forced planar symmetry ($z = 0$ plane), where reflection boundary conditions are implemented.

At $t = 1$ Gyr (panel c, Fig. 5) the $\rm SB_X$ map shows a region of enhanced emission, several kpc in size, close to the centre of the galaxy ($0 \lesssim y \lesssim 5$ kpc). They are caused by relatively dense and cold gas, some of which is actually cooling to low temperatures ($T \lesssim 10^5$ K) and dropped out from the flow (Figure 6, panel a). This is a very interesting phenomenon, because the off-centre cooling might explain the widespread presence of cold ($T \sim 10^4$ K) gas in large ellipticals with conspicuous hot gas (see references quoted in the Introduction). Despite being linearly stable against thermal instability (e.g. Balbus 1988; Balbus & Soker 1989; Loewenstein 1989; Malagoli et al. 1990), the non-conducting hot gas may well cool if the amplitude of the perturbations is sufficiently large (Reale et al. 1991; Yoshida et al. 1991; McCourt et al. 2012; Sharma et al. 2012). High resolution

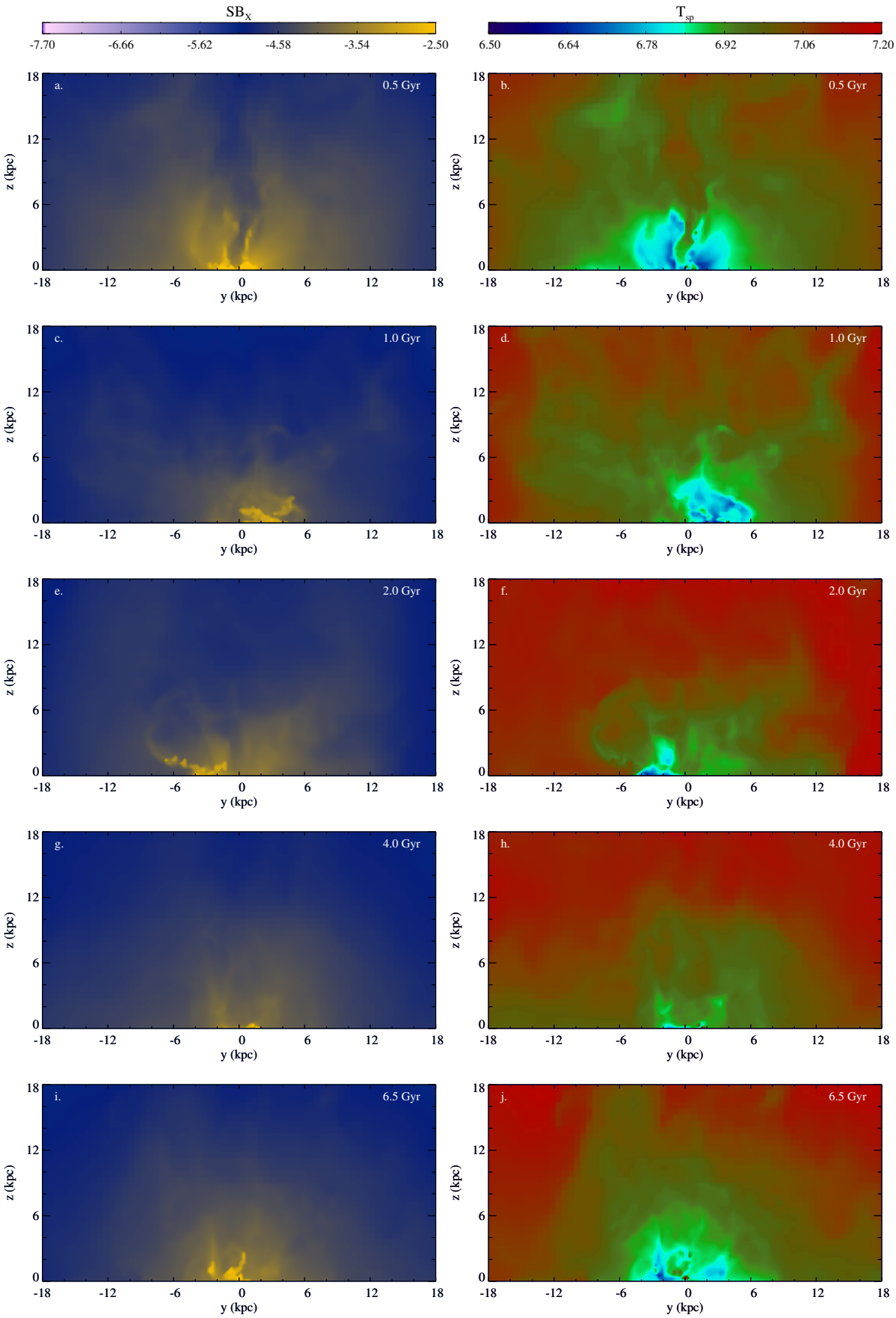

Figure 5. Maps of X-ray surface brightness (left) and projected spectroscopic-like temperature (right) for the best model with circumgalactic gas (cgg-8em4), at five different times (from top to bottom row): 0.5, 1.0, 2.0, 4.0, and 6.5 Gyr. See Section 4.1.1.

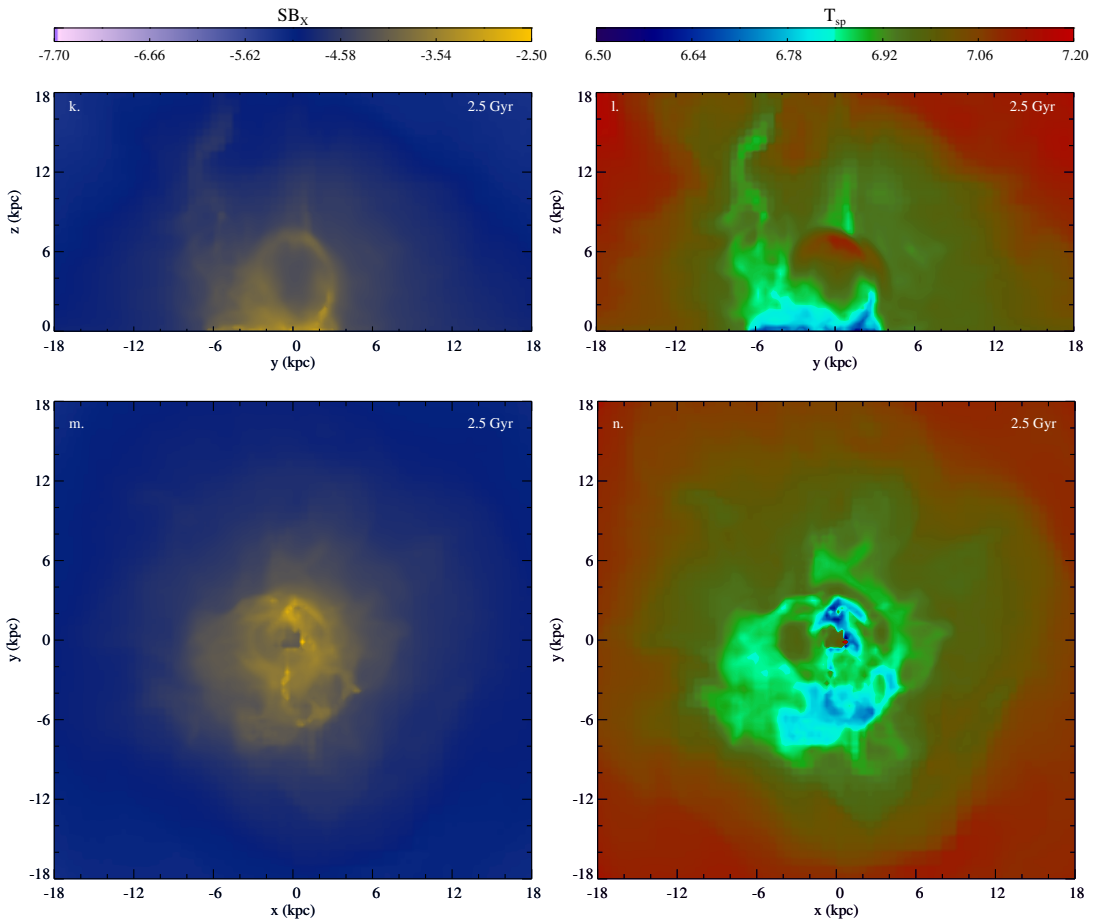

Figure 5. *Continued.* For time 2.5 Gyr we present both the x-axis (top) and z-axis (bottom) projection of the $\mathrm{SB_X}$ and $T_{\rm sp}$ map.

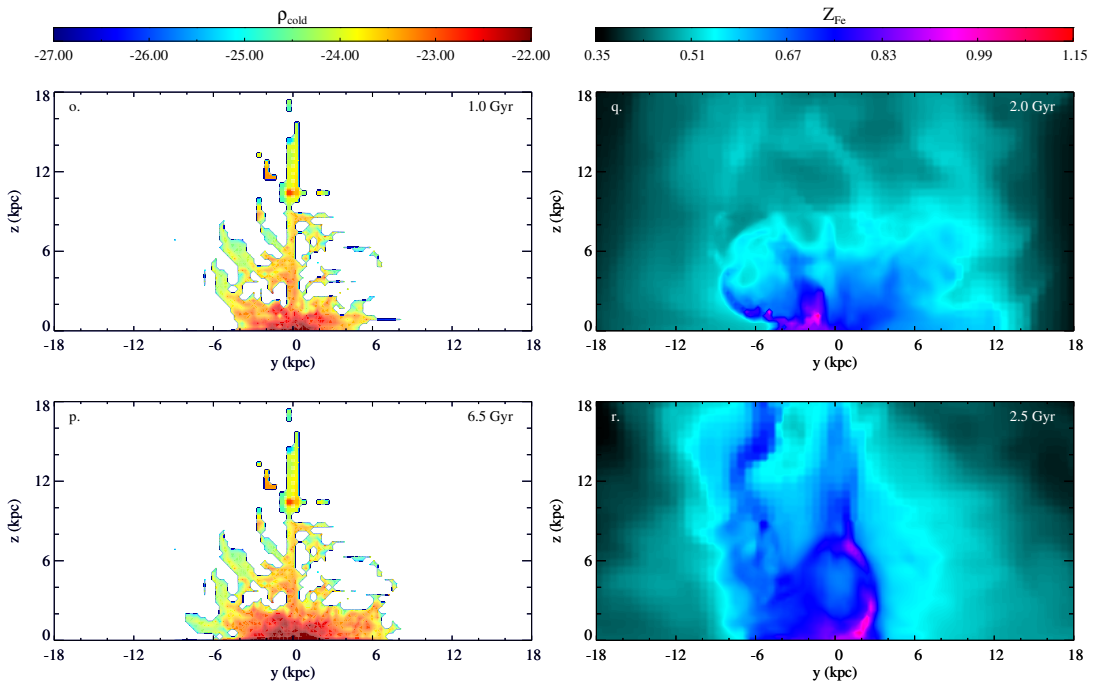

Figure 6. Maps of total dropped cold gas ($T \leqslant 2 \times 10^4$ K; left) and emission-weighted iron abundance (right), both projected along the x-axis, for model cgg-8em4 at different times; see Section 4.1.1.

X-ray maps show indeed a wealth of irregularities in the hot gas, which certainly imply large perturbations in the gas density. Localised gas density enhancements are naturally generated in regions of converging flows, resulting in local cooling times much lower than the free-fall times. This allows the gas to reach very low temperatures, $T \approx 5 \times 10^4$ K, when it is removed from the grid (see also Brighenti & Mathews 2002). The process of multiphase gas formation (in cluster cores heated by AGN jets) has been investigated in depth by our recent work, Gaspari et al. (2012), showing that the non-linear perturbations, associated with the AGN jet feedback, commonly induce the condensation of hot gas into a cold filamentary phase (as also indicated by Figure 6, left panels).

Cooling gas at large distance from the galactic centre is seen also at $t = 2$ Gyr (panel e), in an enhanced SB_X region defined by $z \lesssim 1$ kpc and $R \lesssim 7$ kpc. Several cavities surrounded by relatively cold, bright rims buoyantly rise on various scales (panel f), while very weak shocks rapidly vanish as sound waves at large radii. The cold rims are metal rich, as expected, being formed by gas originally at the centre of the galaxy. In the present model, in fact, we followed the chemical enrichment of the hot gas halo, with emphasis on the evolution of the iron expelled by SNIa. The map of the (emission-weighted) iron abundance is shown in Figure 6 (panel b). The AGN outflows generate asymmetries in the Fe distribution: the relatively metal-rich gas originally in the centre is uplifted along the direction of the outflow and cavities. This results in regions of enhanced iron abundance (by $20 - 30\%$) which trace the dynamics of the recent outflows. Beside this global behaviour, kpc-sized inhomogeneities are also evident in the abundance map.

At $t = 4$ Gyr (panels g and h) a complex structure is visible in the X-ray surface brightness image, mainly due to the generation of multiple cavities and bright filaments. As usual, brightness contrasts are accompanied by temperature and metallicity variations, here on the order of 10%. These images show that the recurrent AGN outflows naturally generate and drive turbulence in the core, with typical velocities of few hundreds km s^{-1} (see Section 5.1.1). The chaotic turbulent environment naturally produces the complex irregular features, at the same time increasing the level of thermalisation in the central region via jet fragmentation.

At $t = 6.5$ Gyr (panels i and j), almost at the end of the simulation, we observe irregular regions of high surface brightness in the central few kpc, where the gas cools to very low temperatures producing diffuse Hα emission. Figure 6 (panel c) provides the total dropped cold mass (integrated in time), indicating again that the cold phase condenses out of the hot flow not only at the very centre, but in an extended region of radius $7 - 15$ kpc. Quantifying the amount and distribution of gas cooling far from the centre is a difficult problem (due to numerical diffusion and resolution). Nevertheless, the result is qualitatively robust: off-centre cooling exists, as indicated by observations, and it can be triggered by the AGN feedback process.

We conclude the snapshot analysis for the CGG model showing a textbook example of X-ray cavity confined by bright rims (panels k and l). The largest brightness contrast between the X-ray hole and the rims is about a factor of two. From the spectroscopic-like temperature map we see that the lower part of the rims ($z \lesssim 3$ kpc) are colder, in projection, than the nearby ISM, while the upper part is slightly hotter, because of shock heating. Again, the rims, being originated from central gas, are slightly more metal-rich than the ISM at the same radius, by 15-25% in the iron abundance (Fig. 6, panel d). For this time, we also show the projection along the z-direction (Fig. 5, panels m and n). Several structures and cavities are visible, together with X-ray bright filaments. In this projection the $T_{\rm sp}$ is characterised by an arc-shaped region about $\sim 20\%$ colder than the neighbouring gas. This comparison between two different projections warns how complicated is the interpretation of real data, especially when the inclination of the outflow, with respect to the plane of the sky, is uncertain.

The generation of buoyant bubbles, together with all the previous consistent observational features (extended multiphase gas, metals asymmetries, turbulence, weak shocks), strengthens the key role of mechanical AGN outflows in regulating the thermal and dynamical evolution of elliptical galaxies, with or without circumgalactic gas.

5 DISCUSSION

5.1 AGN feedback in elliptical galaxies

In the previous Sections we have investigated the effect of AGN feedback on the evolution of the ISM in massive elliptical galaxies. In designing the 3D hydrodynamic simulations we have been guided by several ideas.

(i) The AGN feedback in low-redshift elliptical galaxies acts mainly through a (radiatively inefficient) mechanical and directional process, in the form of jets or winds.

(ii) These outflows interact with the ISM and heat the medium on scales of several kpc, as indicated by X-ray observations of cavities and shocks.

(iii) The AGN reacts to gas cooling: cold gas condenses out of the hot phase in the central region, and it is assumed accreted onto the black hole in a few dynamical times, triggering the AGN feedback. The uncertainties on the the real accretion rates force us to adopt a parametrisation as simple as possible (the only governing parameter being the mechanical efficiency ϵ). Given the uncertainties mentioned in Section 2.1.1, we are not in the position to investigate important issues such as the exact BH growth or the details of the AGN duty cycle.

(iv) The feedback mechanism must work for objects of any scale, from isolated galaxies to massive galaxy clusters.

(v) The calculated evolution of the hot gas must be checked against many available observational constraints, for a long time span (several Gyr).

In G11a,b we have shown that AGN outflows are able to solve the cooling flow problem for both massive clusters and groups, for more than 7 Gyr. We are left now to demonstrate that these mechanical massive outflows, self-regulated by cold accretion, represent also the dominant feedback mechanism on the galactic scales.

In Section 3 we have discussed several models for the isolated elliptical, while the more astrophysically relevant case, i.e. the galaxy with circumgalactic gas, is tackled in Section 4. The two key tests that the models must pass are the agreement with the low cooling rates allowed by observations, and the moderate gas temperature in the central

region of galaxies (no overheating). The former sets a lower limit for the feedback mechanical efficiency, the latter provides an upper bound.

In Figures 2 and 4 we showed that assuming an efficiency $\epsilon \gtrsim 3 \times 10^{-4}$ ($\epsilon \gtrsim 8 \times 10^{-4}$) for the isolated (CGG) model, the cooling rate drops to values close the observational limits reported in the Introduction. The previous values for the mechanical efficiency are lower than those working for clusters (G11a) and similar to those quoted in Ciotti & Ostriker (2007), although for a different feedback scheme. Because our estimated accretion rate onto the BH is likely an upper limit, a firm result of our calculations is that the mechanical efficiency must be $\epsilon \gtrsim$ few $\times 10^{-4}$ in order to prevent significant gas cooling in massive elliptical galaxies. It is more difficult to place an upper bound for the efficiency. We have shown in Section 3 that when $\epsilon \gtrsim 10^{-3}$ the AGN feedback is too intense and the ISM in the central region is overheated. However, larger mechanical efficiencies would be allowed if the accretion rate is grossly overestimated in our simulations.

While the exact details of feedback engine (such as the duty cycle) are uncertain and must be investigated by high-resolution, specialised simulations, the astrophysically most relevant and solid result of this work is that AGN outflows can *solve the cooling flow problem* also in elliptical galaxies, drastically quenching the cooling rates and properly maintaing a quasi thermal equilibrium in the core. This is a remarkable result, given the difficulties encountered with purely thermal feedback (regardless of its origin, i.e. artificially inflated bubbles or radiative heating).

They also agree with a number of other key and independent observational constraints, as illustrated in Sections 3 and 4. A crucial requirement for an AGN feedback scenario is the ability to produce (weak) shocks, X-ray cavities and abundance inhomogeneities, common features shown in deep X-ray observations (see references in the Introduction). These properties point toward a feedback mechanism able to distribute energy and momentum in a directional way, on scales of several kpc. Observationally, these ISM perturbations are best studied in X-ray bright objects, often giant ellipticals with CGG or groups. About 25-50% of galaxies/groups observed at high resolution show evidence of cavities (McNamara & Nulsen 2007; Dong et al. 2010), a number likely underestimated. In galaxy clusters the detection fraction rises to $\gtrsim 2/3$ (Dunn & Fabian 2006). Moreover, cavities are more likely present in cool-core systems (Dong et al. 2010), implying that the feedback action must preserve the positive temperature gradients. Elliptical weak shocks are also commonly found (Gitti et al. 2012), surrounding stable buoyant cavities, a natural by-product of jets and outflows (G11a,b).

In Sections 3.4.1 and 4.1.1 we have illustrated the wealth of observable features created by the (anisotropic) mechanical feedback scenario. Deep X-ray observations of galaxies (e.g. NGC 4472, Biller et al. 2004; NGC 4374, Finoguenov et al. 2008; NGC 4636, Baldi et al. 2009) and groups (e.g. NGC 5044, David et al. 2009; HCG 62, Gitti et al. 2010; NGC 5813, Randall et al. 2011; NGC 5836, Machacek et al. 2011) reveal a wealth of features certainly linked to the AGN feedback outbursts. In particular, the two typical fingerprints naturally left by collimated AGN outflows, i.e. X-ray cavities surrounded by a weak shock, are seen in many snapshots of Figures 3 and 5, often resembling observations also from a quantitative point of view (e.g. elliptical cocoons, Mach number, bubble size and temperature). It is impossible to make a 1:1 comparison with real objects, catching the exact evolutionary moment, with the same instantaneous feedback values. Unfortunately, we are not in the position to calculate the time fraction in which the simulated cavities or shocks are visible; this would in fact require an analysis of the flow very finely spaced in time – subject of a future investigation.

Typically, the cavities inflated by the outflows have size of few kpc and are surrounded by bright rims (e.g. Figure 3, $t = 3.75$, 4.25, and 11.75 Gyr; Figure 5, $t = 0.5$, 2.0, 2.5, and 4.0 Gyr). The rims are often slightly cooler and metal-richer compared to the nearby gas, although there are few exceptions. It is worth mentioning that dedicated simulations tailored for NGC 4636, indicate that it is possible to explain most of the properties of the cavities detected in NGC 4636, assuming the feedback proposed in this work (Ballone & Brighenti, in preparation).

In the case of the galaxy with CGG (similar to a group environment), the frequent activity of the AGN causes the common presence of a low-density channel along the $z-$direction carved by the outflows, $\lesssim 1$ kpc wide and several kpc long. This feature is very difficult to detect in the surface brightness map. In Figure 5 we see that only at the beginning of the calculation, at $t = 0.5$ kpc, the tunnel is visible, with a brightness contrast of $\sim 2-3$ (rapidly decreasing beyond $z = 5$ kpc). Most of the time, the thin channel is wiped out in the brightness image by projection effects (see also G11b). Occasionally, the tunnel may resemble a X-ray cavity (Fig. 5, $t = 2$ Gyr). A dedicated analysis through a very deep X-ray observation in the core of the galaxy may detect this feature or, at least, set constraints on its presence (see, for instance, the SB_x contours in the inner 3 kpc of NGC 5813, Randall et al. 2011). The channel is nevertheless a transient feature, easily fragmented and destroyed by the AGN turbulence, a key element for a proper deposition and thermalisation of mechanical energy in the core (Sec. 5.1.1).

The proposed AGN feedback mechanism has another impact on the gas cooling process, beside significantly lowering the total rate. It promotes spatially distributed cooling (via thermal instabilities), over an extended region of size $\sim$ 10 kpc centred on the BH. Figure 6, left column, show the density map of total cold gas which has cooled and dropped out of the flow, highlighting both the extended and concentrated toroidal distribution of cooler gas (see also Gaspari et al. 2012). Our code does not follow the dynamics of the cooling gas, but it is plausible that some of the cooled gas accretes on the BH, and some is instead used to form new stars and the emission line nebulae commonly observed in elliptical galaxies (see Introduction). At the moment of cooling, the gas has a chaotic motion, with typical velocities of $100 - 200$ km s^{-1}, concordant with Hα spectroscopic studies (Caon et al. 2000).

The mechanical feedback is also able to reproduce the anisotropic distribution of metals, commonly observed in AGN-heated cores (e.g. Rasmussen & Ponman 2009; David et al. 2011; Kirkpatrick et al. 2011; O'Sullivan et al. 2011a). The powerful mechanical jets can indeed uplift up to $\sim$ 10 kpc the metals processed by SNIa and stellar winds in the

nuclear region (with a peak metallicity of $Z_{\rm Fe} \lesssim 1\ Z_\odot$; Mathews & Brighenti 2003). In the more quiescent phases, AGN turbulence tends instead to stir and diffuse the metals, restoring the homogeneous distribution (Figure 6, right panels).

5.1.1 AGN turbulence

Another test the feedback model must pass, although not stringent as those previously discussed, is the generation of turbulence (or bulk motion) in the ISM, especially in the central region. Deep X-ray observations start to provide reliable estimates on the turbulent pressure (Werner et al. 2009; Sanders et al. 2011; de Plaa et al. 2012). The latter authors, in particular, give estimates of the ISM velocity dispersion in the central $\sim$ 10 kpc for two exemplary groups: $320 < v_{\rm turb} < 720$ km s^{-1} (NGC 5044) and $140 < v_{\rm turb} < 540$ km s^{-1} (NGC 5813). In order to compare the prediction of our CGG model with this observation, we calculate the gas velocity dispersion along the line of sight l, weighted by the emission-measure, as

$$\sigma^2_{\rm turb} = \frac{\int \rho^2 (v_l - \bar{v}_l)^2\, dl}{\int \rho^2\, dl}\,, \qquad (5)$$

where the mean velocity $\bar{v}_l$ is typically very close to zero.

In the (projected) circular region $0 < R < 5$ kpc, the time average velocity dispersion is ~ 200 km s^{-1}, when the system is viewed along the outflow z-axis. In the phases where the AGN is more active $\sigma_{\rm turb}$ can reach values as high as 400 km s^{-1}. Note that the outflow, with velocity often exceeding 10^4 km s^{-1}, poorly contributes to $\sigma_{\rm turb}$, because of the very low density. The gas turbulence becomes weaker at larger distances from the centre. In the ring $5 < R < 20$ kpc, $\sigma_{\rm turb}$ decreases to $\sim 60-100$ km s^{-1}, while in the region $20 < R < 40$ kpc, $\sigma_{\rm turb} \sim 40 - 70$ km s^{-1}. One missing element of our models is the effect of cosmological merging and inflow, which may trigger additional turbulence, although more efficiently at large radii (> 0.1 the virial radius; e.g. Vazza et al. 2011).

When the galaxy is observed along a line of sight perpendicular to the outflow direction (e.g. the $x-$axis) the mean central $\sigma_{\rm turb}$ has lower values, ~ 100 km s^{-1}, with peaks about a factor of two larger. For the standard cooling flow model presented in Section 3.1 we find instead $\sigma_{\rm turb} \lesssim 45$ km s^{-1}. This quantity is certainly not associated with turbulent motions, while it represents the steady radial inflow velocity due to the massive cooling flow.

We conclude that subrelativistic outflows are able to generate the observed turbulent pressure and hot gas velocity dispersions. This non-thermal pressure is generally a fraction of the thermal energy, in the range $5 - 15\%$ ($E_{\rm turb}/E_{\rm th} \approx 0.1\,(v^2_{\rm turb,200}/T_7)$, where the turbulent velocity is expressed in units of 200 km s^{-1}, and the gas temperature in units of 10^7 K).

5.2 Comparison with other AGN feedback scenarios

It is interesting to compare our purely mechanical feedback with other types of AGN heating processes. To our knowledge, only very few investigations focused on AGN feedback in ellipticals. For example, Ciotti, Ostriker and collaborators (1997, 2010) have investigated a type of feedback triggered by AGN radiation (mainly Compton heating, radiation pressure, plus an approximation of a broad-line-region wind), through 1D hydrodynamic simulations. The best models have been analysed in detail by Pellegrini et al. (2012) and compared to observations. The key feature of these models is the formation of a cold shell at $r \sim 1$ kpc, whose evolution governs the whole quasar-like feedback heating (in order to be efficient, radiative feedback requires a very dense - optically thick - absorbing medium). We note that in 1D simulations a cold shell can numerically form under several circumstances, with or without AGN heating (see for instance the 'galactic drip' phenomenon described in Mathews & Brighenti 1997 and Brighenti & Mathews 2002). It is not clear how 1D calculations are able to realistically follow the formation and evolution of the shell. Subsonic, non-radial gas velocity appearing in multidimensional models tend to suppress this feature (Brighenti & Mathews 1997). The cold shell is also Rayleigh-Taylor unstable and should fragment in about a dynamical time, $\sim$ few $\times\, 10^6$ yr. Another complication is the difficulty for hydrodynamic simulations to reproduce the real complexity of the observed multiphase ISM in the inner $<$ kpc (see Introduction).

Given these uncertainties, it seems more appropriate to compare our results with those presented in Novak et al. (2011), where the 2D version of the previous feedback scenario for an isolated elliptical galaxy is investigated. In these simulations conical outflows, representing broad absorption line (BAL) winds, are generated near the centre of the grid, making the computed scenario qualitatively similar to our models. Novak et al. (2011) found that the accretion process significantly changes in 2D, reducing the effectiveness of the feedback mechanism with respect to isotropic 1D models. They explored the effect of varying the mechanical efficiency, finding that an acceptable BH growth is attained when $\epsilon \gtrsim 10^{-4}$, consistent with the preferred values found in our work. About $10^{10}\ M_\odot$ of stars form in Novak's ellipticals, almost independently on the wind efficiency, implying a mean star formation rate of $\sim 0.8\ M_\odot$ yr^{-1}. It would be interesting to estimate the central Balmer indexes (dependent on the star formation history) and compare them with the available observations (e.g. Kuntschner et al. 2010).

Unfortunately, Novak et al. (2011) do not show azimuthally averaged temperature and density profiles, thus it is not possible to assess the effect of the AGN feedback on these key observable constraints. Nevertheless, together with our calculations, the results presented in Novak et al. (2011) corroborate the potential importance of bipolar outflows as a primary source of AGN feedback.

Debuhr et al. (2011) carried out 3D SPH simulations of AGN outflows driven by quasar radiation during a major merger. They noted that radiation pressure alone does not produce any substantial feedback, requiring an additional momentum kick with velocity $\sim 10^4$ km s^{-1} (like BAL winds), similar to our best models. Large values of the optical depth are usually required to boost such fast outflows ($\tau \sim 5 - 10$). The strong isotropic outburst produces a clear galactic outflow, drastically reducing the mass inside 3 kpc (two orders of magnitude). This is a typically feature associated with strong isotropic heating (either mechanical or thermal), which unbinds and shocks the central gas to

unobserved levels in normal ellipticals. Bipolar mechanical outflows are instead gentler, capable to reproduce the observed anisotropic X-ray features as cavities (Figure 3).

As a concluding remark, we note that the radiative feedback displays a strong impact on the ISM only in the presence of quasar-like objects, which are certainly rare in the local universe, with a rapid decline below redshift ~ 1.8 (Schneider et al. 2005).

5.3 Comparison with galaxy clusters and groups

After a systematic study of AGN outflow feedback, from the cluster scales down to the galactic systems (Gaspari et al. 2009, 2011a,b, 2012), it is worth to wrap-up and emphasise the main similitudes and differences.

Despite the very different environments of clusters, groups and ellipticals, purely mechanical AGN feedback, in the form of massive anisotropic outflows, is anyway able to suppress the cooling flow down to a factor $\lesssim 5-10\%$. The self-regulation process is fundamental for preserving the cool-core structure, in a state of quasi thermal equilibrium.

In order to have a proper self-regulation, the AGN feedback seems to require mechanical efficiencies decreasing with the halo mass: $\epsilon \sim 5\times10^{-3}$ (cluster), $\sim 8\times10^{-4}$ (group) and $\sim 3\times10^{-4}$ (isolated elliptical). We stress that this ϵ does not probably represent the actual real efficiency. The accreted mass on the black hole may be lower, while the feedback power could be maintained on the same level by increasing the efficiency. Nevertheless, the increasing efficiency with system mass trend could be real. In fact, the same mechanical feedback successful in massive clusters ($M_{\rm vir}\sim10^{15}$ $M_\odot$) needs to work on a relatively less powerful regime in order to prevent the core disruption in groups or galaxies ($\lesssim 4\times10^{13}$ $M_\odot$), which are less bound objects. Even with a lower ϵ, the feedback in lighter halos has still more dramatic consequences on the temperature and density profiles, with the stronger outbursts easily perturbing the central region. The isolated galaxy is the exemplary case, in which single outflows of power $\sim 10^{44}$ erg s^{-1} and $\epsilon = 3.3\times10^{-4}$ can eject the gas outside the small system, stopping cooling for several tens Myr. Applying a feedback 20 times stronger, as required for clusters, would eject the whole ISM and empty the galaxy for several Gyr. The physical reason for the mechanical efficiency to be linked to the environment/potential well is unclear and needs to be clarified with future investigations.

The cooling flow problem in our simulations is solved through AGN outflows for more than 7-10 Gyr, despite the exact details of the feedback mechanism (cf. G11a and Gaspari et al. 2012). In the cluster calculations the resulting feedback was impulsive, with strong outbursts sometimes exceeding Eddington power. Increasing the resolution leads to a higher outflow frequency (and lower powers), because the central inflowing material is able to accrete more easily along the direction perpendicular to the jet axis. The AGN outburst frequency is also correlated to the efficiency, e.g. in the group the outflow injection is almost continuous with a duty cycle around 0.8. The isolated galaxy is a slightly different case, because the absence of the circumgalactic gas helps the feedback action, leading to a mildly impulsive behaviour.

The galaxy simulation cgg-8em4 (Sec. 4) can be regarded as a convergence test of the best feedback group model in G11b. The increase in resolution is almost a factor 2 and we find indeed consistent results. Cooling rates and profiles are similar, concordant with observational data. Also the jet powers ($\sim 3-5\times10^{44}$ erg s^{-1}) are similar, showing an analogous evolutionary pattern and frequency. It is worth noting that the jet active region is $R\times z\simeq 1\times1$ kpc in the CGG model, while 1×2 kpc in the group run presented in G11b. Therefore, a slightly longer jet does not alter the feedback properties (the same can be said for the width, as tested in previous models).

In all the best models the self-regulated outflow velocities are around 10^4 km s^{-1}, with rarer events reaching several 10^4-10^5 km s^{-1} in the strongest phases. The mean mass outflow rate decreases with the mass of the system: several tens $M_\odot$ yr^{-1} (cluster), few $M_\odot$ yr^{-1} (group), and $\lesssim 1$ $M_\odot$ yr^{-1} (isolated galaxy). More massive and slower outflows usually show a higher piercing power, producing a narrow unidirectional channel. This is more evident in almost continuous feedback models, like galaxy groups or galaxies with CGG. However, the projected X-ray surface brightness maps mask this narrow feature (~ 1 kpc) most of the times. Moreover, the turbulence generated by the feedback can easily alter and fragment the jet path, producing tiny bubbles. On the contrary, relatively lighter and faster outflows (still subrelativistic) thermalise the energy more efficiently, inflating big buoyant bubbles.

In the cluster regime the bubbles have usually a radius of few tens kpc, with emission-weighted temperatures slightly hotter than the ambient medium; the reduced power in groups and ellipticals produces more 'delicate' cavities (with radius several and few kpc, respectively), showing relatively cold rims and mild internal temperatures; the jump in SB_X is typically $20-40\%$. In all three systems, different or fragmented jet outbursts generate also a series of weak shocks with Mach number $1.1-1.3$, visible as faint ripples in the temperature and brightness profiles. Another fundamental feature they all have in common is the uplift of relatively cold and metal-rich gas, in particular during more powerful episodes, which creates an asymmetrical distribution in the iron abundance map ($10-20\%$ contrast with the background).

The most successful models are those where the accretion is linked to cold gas. Hot gas accretion, based on the original Bondi prescription, usually provides accretion rates one or two orders of magnitude lower, requiring very high mechanical efficiencies, $\epsilon\gtrsim 0.1$, in order to make the feedback effective. Moreover, its continuous nature poses serious doubts on the cyclic production of typical features, such as buoyant cavities. Linking the accretion to the cooling rate induces instead a natural self-regulation, with some kind of recursive cycle and peaks of activity. The success of the feedback is essentially independent of the dropout parameters, such as $T_{\rm cut}$ (e.g. 2×10^4 or 5×10^5 K), the dropout function (exponential or step), or the delay associated with the free fall of cold blobs. The simulations carried out in Gaspari et al. (2012), with the accretion traced only by the inflow in the nuclear region, confirm that the bulk of AGN fuelling is associated with the cold – and not hot – phase (check $M_{\rm acc}$ in fig. 3).

6 CARDINAL CONCLUSIONS

For all the reasons argued above and based also on our previous theoretical numerical studies on AGN heating, we find that the best feedback mechanism able to *solve the cooling flow problem* in every virialised system with a substantial hot gas halo, requiring

- no overcooling ($\dot{M}_{\rm cool} < 5 - 10\%\ \dot{M}_{\rm classic\,CF}$),
- no overheating (preserve the cool-core structure),

and reproducing several observational features, such as

- buoyant underdense bubbles,
- elliptical cocoons,
- weak shocks/sonic ripples (Mach $\lesssim 1.5$),
- dredge-up of metals and cold gas,
- subsonic turbulence (hundreds km s^{-1}),
- extended filamentary and nuclear cold gas,

should possess the following key characteristics:

- mechanical,
- anisotropic,
- driven by massive and subrelativistic outflows,
- self-regulated by cold accretion,
- and less efficient in lighter halos.

ACKNOWLEDGMENTS

The software used in this work was in part developed by the DOE NNSA-ASC OASCR Flash Center at the University of Chicago. We acknowledge the NASA awards SMD-10-1609, SMD-11-2209 (Pleiades), and the CINECA awards HP10BPTM62, HP10BOB5U6 (SP6). Partial support for this work was provided by NASA under grant NNH09ZDA001N, issued through the Office of Space Sciences Astrophysics Data Analysis Program.

REFERENCES

Balbus S. A., 1988, ApJ, 328, 395
Balbus S. A., Soker N., 1989, ApJ, 341, 611
Baldi A., Forman W., Jones C., Kraft R., Nulsen P., Churazov E., David L., Giacintucci S., 2009, ApJ, 707, 1034
Balogh M. L., Babul A., Voit G. M., McCarthy I. G., Jones L. R., Lewis G. F., Ebeling H., 2006, MNRAS, 366, 624
Benson A. J., Bower R. G., Frenk C. S., Lacey C. G., Baugh C. M., Cole S., 2003, ApJ, 599, 38
Beuing J., Dobereiner S., Bohringer H., Bender R., 1999, MNRAS, 302, 209
Biller B. A., Jones C., Forman W. R., Kraft R., Ensslin T., 2004, ApJ, 613, 238
Binney J., Tabor G., 1995, MNRAS, 276, 663
Böhringer H., Werner N., 2010, A&A Rev., 18, 127
Booth C. M., Schaye J., 2009, MNRAS, 398, 53
Bregman J. N., Fabian A. C., Miller E. D., Irwin J. A., 2006, ApJ, 642, 746
Bregman J. N., Miller E. D., Athey A. E., Irwin J. A., 2005, ApJ, 635, 1031
Bregman J. N., Miller E. D., Irwin J. A., 2001, ApJ, 553, L125
Bregman J. N., Parriott J. R., 2009, ApJ, 699, 923
Brighenti F., Mathews W. G., 1997, ApJ, 490, 592
Brighenti F., Mathews W. G., 1998, ApJ, 495, 239
Brighenti F., Mathews W. G., 2002, ApJ, 573, 542
Brighenti F., Mathews W. G., 2003, ApJ, 587, 580
Brighenti F., Mathews W. G., 2006, ApJ, 643, 120
Brighenti F., Mathews W. G., 1999, ApJ, 512, 65
Brüggen M., Heinz S., Roediger E., Ruszkowski M., Simionescu A., 2007, MNRAS, 380, L67
Brüggen M., Ruszkowski M., Hallman E., 2005, ApJ, 630, 740
Bullock J. S., Kolatt T. S., Sigad Y., Somerville R. S., Kravtsov A. V., Klypin A. A., Primack J. R., Dekel A., 2001, MNRAS, 321, 559
Buote D. A., Brighenti F., Mathews W. G., 2004, ApJ, 607, L91
Buote D. A., Lewis A. D., Brighenti F., Mathews W. G., 2003, ApJ, 594, 741
Buson L. M. et al., 1993, A&A, 280, 409
Caon N., Macchetto D., Pastoriza M., 2000, ApJS, 127, 39
Cappellaro E., Evans R., Turatto M., 1999, A&A, 351, 459
Cappi M., Giustini M., Tombesi F., 2011, in The X-ray Universe 2011, J.-U. Ness & M. Ehle, ed., p. 51
Cappi M. et al., 2009, A&A, 504, 401
Cattaneo A. et al., 2009, Nature, 460, 213
Cattaneo A., Teyssier R., 2007, MNRAS, 376, 1547
Churazov E., Sazonov S., Sunyaev R., Forman W., Jones C., Böhringer H., 2005, MNRAS, 363, L91
Ciotti L., D'Ercole A., Pellegrini S., Renzini A., 1991, ApJ, 376, 380
Ciotti L., Ostriker J. P., 1997, ApJ, 487, L105
Ciotti L., Ostriker J. P., 2007, ApJ, 665, 1038
Colbert J. W., Mulchaey J. S., Zabludoff A. I., 2001, AJ, 121, 808
Crenshaw D. M., Kraemer S. B., George I. M., 2003, ARA&A, 41, 117
Croton D. J. et al., 2006, MNRAS, 365, 11
Dalla Vecchia C., Bower R. G., Theuns T., Balogh M. L., Mazzotta P., Frenk C. S., 2004, MNRAS, 355, 995
David L. P., Forman W., Jones C., 1991, ApJ, 380, 39
David L. P., Jones C., Forman W., Daines S., 1994, ApJ, 428, 544
David L. P., Jones C., Forman W., Nulsen P., Vrtilek J., O'Sullivan E., Giacintucci S., Raychaudhury S., 2009, ApJ, 705, 624
David L. P., Jones C., Forman W., Vargas I. M., Nulsen P., 2006, ApJ, 653, 207
David L. P. et al., 2011, ApJ, 728, 162

de Plaa J., Zhuravleva I., Werner N., Kaastra J. S., Churazov E., Smith R. K., Raassen A. J. J., Grange Y. G., 2012, arXiv:astro-ph/1201.1910
Debuhr J., Quataert E., Ma C.-P., 2011, MNRAS, 2150
Di Matteo T., Allen S. W., Fabian A. C., Wilson A. S., Young A. J., 2003, ApJ, 582, 133
Diehl S., Statler T. S., 2008a, ApJ, 680, 897
Diehl S., Statler T. S., 2008b, ApJ, 687, 986
Dong R., Rasmussen J., Mulchaey J. S., 2010, ApJ, 712, 883
Dubois Y., Devriendt J., Slyz A., Teyssier R., 2010, MNRAS, 409, 985
Dunn J. P. et al., 2010a, ApJ, 709, 611
Dunn R. J. H., Allen S. W., Taylor G. B., Shurkin K. F., Gentile G., Fabian A. C., Reynolds C. S., 2010b, MNRAS, 404, 180
Dunn R. J. H., Fabian A. C., 2006, MNRAS, 373, 959
Ellis S. C., O'Sullivan E., 2006, MNRAS, 367, 627
Eskridge P. B., Fabbiano G., Kim D.-W., 1995, ApJS, 97, 141
Fabian A. C., 1994, ARA&A, 32, 277
Fabian A. C., Rees M. J., 1995, MNRAS, 277, L55
Ferrarese L., Merritt D., 2000, ApJ, 539, L9
Ferrari F., Pastoriza M. G., Macchetto F., Caon N., 1999, A&AS, 136, 269
Ferreras I., Silk J., 2000, ApJ, 541, L37
Finoguenov A., Ruszkowski M., Jones C., Brüggen M., Vikhlinin A., Mandel E., 2008, ApJ, 686, 911
Fryxell B. et al., 2000, ApJS, 131, 273
Fukazawa Y., Botoya-Nonesa J. G., Pu J., Ohto A., Kawano N., 2006, ApJ, 636, 698
Gaspari M., Melioli C., Brighenti F., D'Ercole A., 2009, in AIP Conf. Series, Vol. 1201, The Monsters Fiery Breath: Feedback in Galaxies, S. Heinz & E. Wilcots, ed., pp. 309–312
Gaspari M., Melioli C., Brighenti F., D'Ercole A., 2011a, MNRAS, 411, 349, [G11a]
Gaspari M., Brighenti F., D'Ercole A., Melioli C., 2011b, MNRAS, 415, 1549, [G11b]
Gaspari M., Ruszkowski M., Sharma P., 2012, ApJ, 746, 94
Gastaldello F., Buote D. A., Temi P., Brighenti F., Mathews W. G., Ettori S., 2009, ApJ, 693, 43
Gebhardt K. et al., 2000, ApJ, 539, L13
Giacintucci S. et al., 2011, ApJ, 732, 95
Giovannini G., 2004, Ap&SS, 293, 1
Gitti M., Brighenti F., McNamara B. R., 2012, Adv. in Astronomy, 2012, 1
Gitti M., O'Sullivan E., Giacintucci S., David L. P., Vrtilek J., Raychaudhury S., Nulsen P. E. J., 2010, ApJ, 714, 758
Goudfrooij P., Hansen L., Jorgensen H. E., Norgaard-Nielsen H. U., 1994, A&AS, 105, 341
Graves G. J., Faber S. M., Schiavon R. P., 2009, ApJ, 698, 1590
Greggio L., 2005, A&A, 441, 1055
Guo F., Mathews W. G., 2010, ApJ, 712, 1311
Heckman T. M., Baum S. A., van Breugel W. J. M., McCarthy P., 1989, ApJ, 338, 48
Heinz S., Brüggen M., Friedman S., 2011, ApJS, 194, 21
Humphrey P. J., Buote D. A., 2006, ApJ, 639, 136
Humphrey P. J., Buote D. A., Gastaldello F., Zappacosta L., Bullock J. S., Brighenti F., Mathews W. G., 2006, ApJ, 646, 899
Igumenshchev I. V., 2006, ApJ, 649, 361
Irwin J. A., Sarazin C. L., Bregman J. N., 2002, ApJ, 570, 152
Jeong H. et al., 2009, MNRAS, 398, 2028
Jones C., Forman W., Vikhlinin A., Markevitch M., David L., Warmflash A., Murray S., Nulsen P. E. J., 2002, ApJ, 567, L115
Khosroshahi H. G., Jones L. R., Ponman T. J., 2004, MNRAS, 349, 1240
Kim D.-W., Fabbiano G., 2003, ApJ, 586, 826
King A. R., Pringle J. E., 2007, MNRAS, 377, L25
Kirkpatrick C. C., McNamara B. R., Cavagnolo K. W., 2011, ApJ, 731, L23
Krumholz M. R., McKee C. F., Klein R. I., 2005, ApJ, 618, 757
Krumholz M. R., McKee C. F., Klein R. I., 2006, ApJ, 638, 369
Kuntschner H. et al., 2010, MNRAS, 408, 97
Loewenstein M., 1989, MNRAS, 238, 15
Loewenstein M., Mathews W. G., 1987, ApJ, 319, 614
Loewenstein M., Mushotzky R. F., Angelini L., Arnaud K. A., Quataert E., 2001, ApJ, 555, L21
Macchetto F., Pastoriza M., Caon N., Sparks W. B., Giavalisco M., Bender R., Capaccioli M., 1996, A&AS, 120, 463
MacDonald J., Bailey M. E., 1981, MNRAS, 197, 995
Machacek M., Nulsen P. E. J., Jones C., Forman W. R., 2006, ApJ, 648, 947
Machacek M. E., Jerius D., Kraft R., Forman W. R., Jones C., Randall S., Giacintucci S., Sun M., 2011, ApJ, 743, 15
Malagoli A., Rosner R., Fryxell B., 1990, MNRAS, 247, 367
Mannucci F., Della Valle M., Panagia N., Cappellaro E., Cresci G., Maiolino R., Petrosian A., Turatto M., 2005, A&A, 433, 807
Martel A. R., Turner N. J., Sparks W. B., Baum S. A., 2000, ApJS, 130, 267
Mathews W. G., 1990, ApJ, 354, 468
Mathews W. G., 2009, ApJ, 695, L49
Mathews W. G., Baker J. C., 1971, ApJ, 170, 241
Mathews W. G., Brighenti F., 1997, in Astronomical Society of the Pacific Conference Series, Vol. 116, The Nature of Elliptical Galaxies; 2nd Stromlo Symposium, M. Arnaboldi, G. S. Da Costa, & P. Saha, ed., p. 405
Mathews W. G., Brighenti F., 2003, ARA&A, 41, 191
Mathews W. G., Brighenti F., 2008, ApJ, 685, 128
Mathews W. G., Brighenti F., Faltenbacher A., Buote D. A., Humphrey P. J., Gastaldello F., Zappacosta L., 2006, ApJ, 652, L17
Mathews W. G., Faltenbacher A., Brighenti F., Buote D. A., 2005, ApJ, 634, L137
Mathews W. G., Loewenstein M., 1986, ApJ, 306, L7
McConnell N. J., Ma C.-P., Gebhardt K., Wright S. A., Murphy J. D., Lauer T. R., Graham J. R., Richstone D. O., 2011, Nature, 480, 215
McCourt M., Sharma P., Quataert E., Parrish I. J., 2012, MNRAS, 419, 3319
McNamara B. R., Nulsen P. E. J., 2007, ARA&A, 45, 117
Mellier Y., Mathez G., 1987, A&A, 175, 1
Merloni A., Heinz S., 2008, MNRAS, 388, 1011
Moe M., Arav N., Bautista M. A., Korista K. T., 2009, ApJ, 706, 525

Morganti R., Holt J., Saripalli L., Oosterloo T. A., Tadhunter C. N., 2007, A&A, 476, 735
Mościbrodzka M., Proga D., 2008, ApJ, 679, 626
Mościbrodzka M., Proga D., 2009, MNRAS, 397, 2087
Nagino R., Matsushita K., 2009, A&A, 501, 157
Narayan R., Fabian A. C., 2011, MNRAS, 415, 3721
Narayan R., McClintock J. E., 2008, New A Rev., 51, 733
Navarro J. F., Frenk C. S., White S. D. M., 1996, ApJ, 462, 563
Nesvadba N. P. H., Lehnert M. D., De Breuck C., Gilbert A. M., van Breugel W., 2008, A&A, 491, 407
Novak G. S., Ostriker J. P., Ciotti L., 2011, ApJ, 737, 26
Oegerle W. R., Hill J. M., 2001, AJ, 122, 2858
Omma H., Binney J., Bryan G., Slyz A., 2004, MNRAS, 348, 1105
Ostriker J. P., Choi E., Ciotti L., Novak G. S., Proga D., 2010, ApJ, 722, 642
O'Sullivan E., Giacintucci S., David L. P., Vrtilek J. M., Raychaudhury S., 2011a, MNRAS, 411, 1833
O'Sullivan E., Worrall D. M., Birkinshaw M., Trinchieri G., Wolter A., Zezas A., Giacintucci S., 2011b, MNRAS, 416, 2916
Parriott J. R., Bregman J. N., 2008, ApJ, 681, 1215
Pellegrini S., Ciotti L., Ostriker J. P., 2012, ApJ, 744, 21
Peterson J. R., Fabian A. C., 2006, Phys. Rep., 427, 1
Peterson J. R., Kahn S. M., Paerels F. B. S., Kaastra J. S., Tamura T., Bleeker J. A. M., Ferrigno C., Jernigan J. G., 2003, ApJ, 590, 207
Peterson J. R. et al., 2001, A&A, 365, L104
Piontek F., Steinmetz M., 2011, MNRAS, 410, 2625
Pizzolato F., Soker N., 2005, ApJ, 632, 821
Pope E. C. D., 2007, MNRAS, 381, 741
Pope E. C. D., 2009, MNRAS, 395, 2317
Puchwein E., Sijacki D., Springel V., 2008, ApJ, 687, L53
Quataert E., Narayan R., 2000, ApJ, 528, 236
Randall S. W. et al., 2011, ApJ, 726, 86
Rasmussen J., Ponman T. J., 2009, MNRAS, 399, 239
Reale F., Rosner R., Malagoli A., Peres G., Serio S., 1991, MNRAS, 251, 379
Sanders J. S., Fabian A. C., Smith R. K., 2011, MNRAS, 410, 1797
Sansom A. E., O'Sullivan E., Forbes D. A., Proctor R. N., Davis D. S., 2006, MNRAS, 370, 1541
Sarazin C. L., Ashe G. A., 1989, ApJ, 345, 22
Sarazin C. L., Irwin J. A., Bregman J. N., 2001, ApJ, 556, 533
Sarazin C. L., White, III R. E., 1988, ApJ, 331, 102
Sarzi M. et al., 2006, MNRAS, 366, 1151
Sarzi M. et al., 2010, MNRAS, 402, 2187
Schneider D. P. et al., 2005, AJ, 130, 367
Sharma P., McCourt M., Quataert E., Parrish I. J., 2012, MNRAS, 2294
Shields J. C., 1991, AJ, 102, 1314
Sijacki D., Springel V., Di Matteo T., Hernquist L., 2007, MNRAS, 380, 877
Soker N., Pizzolato F., 2005, ApJ, 622, 847
Springel V., Di Matteo T., Hernquist L., 2005, MNRAS, 361, 776
Sutherland R. S., Dopita M. A., 1993, ApJS, 88, 253
Tamura T., Kaastra J. S., Makishima K., Takahashi I., 2003, A&A, 399, 497
Taylor G. B., Sanders J. S., Fabian A. C., Allen S. W., 2006, MNRAS, 365, 705
Temi P., Brighenti F., Mathews W. G., 2009, ApJ, 707, 890
Tombesi F., Cappi M., Reeves J. N., Braito V., 2012, arXiv:astro-ph/1201.1897
Tombesi F., Cappi M., Reeves J. N., Palumbo G. G. C., Yaqoob T., Braito V., Dadina M., 2010a, A&A, 521, A57
Tombesi F., Sambruna R. M., Reeves J. N., Braito V., Ballo L., Gofford J., Cappi M., Mushotzky R. F., 2010b, ApJ, 719, 700
Tornatore L., Borgani S., Springel V., Matteucci F., Menci N., Murante G., 2003, MNRAS, 342, 1025
Trager S. C., Faber S. M., Worthey G., González J. J., 2000, AJ, 119, 1645
Tran H. D., Tsvetanov Z., Ford H. C., Davies J., Jaffe W., van den Bosch F. C., Rest A., 2001, AJ, 121, 2928
Trinchieri G. et al., 2008, ApJ, 688, 1000
Vazza F., Brunetti G., Gheller C., Brunino R., Brüggen M., 2011, A&A, 529, A17
Verdoes Kleijn G. A., Baum S. A., de Zeeuw P. T., O'Dea C. P., 2002, AJ, 123, 1334
Vernaleo J. C., Reynolds C. S., 2006, ApJ, 645, 83
Vikhlinin A., 2006, ApJ, 640, 710
Werner N., Zhuravleva I., Churazov E., Simionescu A., Allen S. W., Forman W., Jones C., Kaastra J. S., 2009, MNRAS, 398, 23
Xu H. et al., 2002, ApJ, 579, 600
Yoshida T., Habe A., Hattori M., 1991, MNRAS, 248, 630
Zanni C., Murante G., Bodo G., Massaglia S., Rossi P., Ferrari A., 2005, A&A, 429, 399